Cell. Mol. Life Sci. (2017) 74:2851–2874
DOI 10.1007/s00018-017-2541-x

Cellular and Molecular Life Sciences

ORIGINAL ARTICLE

Synthetic alpha-synuclein fibrils cause mitochondrial impairment and selective dopamine neurodegeneration in part via iNOS-mediated nitric oxide production

Victor Tapias[1,2] · Xiaoping Hu[3,4] · Kelvin C. Luk[5] · Laurie H. Sanders[3,4] · Virginia M. Lee[5] · J. Timothy Greenamyre[3,4,6]

Received: 31 January 2017 / Revised: 20 April 2017 / Accepted: 15 May 2017 / Published online: 22 May 2017

Abstract Intracellular accumulation of α-synuclein (α-syn) are hallmarks of synucleinopathies, including Parkinson's disease (PD). Exogenous addition of pre-formed α-syn fibrils (PFFs) into primary hippocampal neurons induced α-syn aggregation and accumulation. Likewise, intrastriatal inoculation of PFFs into mice and non-human primates generates Lewy bodies and Lewy neurites associated with PD-like neurodegeneration. Herein, we investigate the putative effects of synthetic human PFFs on cultured rat ventral midbrain dopamine (DA) neurons. A time- and dose-dependent accumulation of α-syn was observed following PFFs exposure that also underwent phosphorylation at serine 129. PFFs treatment decreased the expression levels of synaptic proteins, caused alterations in axonal transport-related proteins, and increased H2AX Ser139 phosphorylation. Mitochondrial impairment (including modulation of mitochondrial dynamics-associated protein content), enhanced oxidative stress, and an inflammatory response were also detected in our experimental paradigm. In attempt to unravel a potential molecular mechanism of PFFs neurotoxicity, the expression of inducible nitric oxide synthase was blocked; a significant decline in protein nitration levels and protection against PFFs-induced DA neuron death were observed. Combined exposure to PFFs and rotenone resulted in an additive toxicity. Strikingly, many of the harmful effects found were more prominent in DA rather than non-DA neurons, suggestive of higher susceptibility to degenerate. These findings provide new insights into the role of α-syn in the pathogenesis of PD and could represent a novel and valuable model to study DA-related neurodegeneration.

Keywords Parkinson's disease · Alpha-synuclein fibrils · Dopamine · Mitochondria · Oxidative stress · Neurodegeneration · Inflammation · Rotenone

Electronic supplementary material The online version of this article (doi:10.1007/s00018-017-2541-x) contains supplementary material, which is available to authorized users.

✉ Victor Tapias
vit2013@med.cornell.edu

[1] Present Address: Department of Neurology and Neuroscience, Weill Cornell Medicine, 525 East 68th Street, New York, NY 10065, USA

[2] Feil Family Brain and Mind Research Institute, Weill Cornell Medicine, 1300 York Ave, New York, NY 10065, USA

[3] Department of Neurology, University of Pittsburgh, Pittsburgh, PA 15260, USA

[4] Pittsburgh Institute for Neurodegenerative Diseases, University of Pittsburgh, Pittsburgh, PA 15260, USA

[5] Department of Pathology and Laboratory Medicine, University of Pennsylvania Perelman School of Medicine, Philadelphia, PA 19104, USA

[6] Pittsburgh VA Healthcare System, Pittsburgh, PA 15206, USA

Introduction

Unfolded monomeric alpha-synuclein (α-syn) may undergo conformational changes to form insoluble α-syn fibrils with a predominantly β-sheet secondary structure, thereby affecting its biological activity. *SNCA* gene point mutations or multiplications of the wild-type allele, environmental alterations, other protein or lipid interactions, and post-translational modifications can generate intraneuritic (Lewy neurites) and intraneuronal (Lewy bodies; LB) pathologic inclusions, which contribute to

neurodegeneration in Parkinson's disease (PD) and related α-synucleinopathies [1–5].

It has been reported that synthetic α-syn fibrils (PFFs) can produce LB-like inclusions that are ubiquitin, Hsp70 and 90, and thioflavin-T positive and resemble human LB in neurons. In addition to sedimentation and Triton X-100 extraction, PFFs have been verified by electron microscopy as amyloid fibril structures [6]. PFFs were internalized by cultured neurons—possibly through an adsorptive endocytosis mechanism—and recruited endogenous α-syn to form aggregates akin to PD-like α-syn inclusions [6, 7]. Contrary to cellular α-syn, PFFs per se did not undergo post-translational modifications after internalization. PFFs transmission was conducted from axons to second-order neurons in an anterograde direction although pathology can also be retrogradely propagated [7].

A significant number of studies have revealed that α-syn localizes at or in mitochondria of DA neurons in cell culture systems, midbrain of rodents, and substantia nigra (SN) and striatum of PD human brains and can compromise mitochondrial function [8, 9]. Mitochondrial imported α-syn caused downregulation of complex I activity and exacerbated oxidative stress, which can further increase endogenous α-syn expression levels, thereby initiating a feed-forward cycle [8, 10, 11]. Enhanced levels of α-syn may alter its regulatory effect on synaptic vesicle docking and fusion driving to cytoplasmic enhancement of DA and related free radical damage, a process that stimulates the formation of pathological forms of the protein through a vicious circle [12].

The importance of α-syn in PD pathology is further supported by the role of the protein in eliciting neuroinflammatory responses. α-Syn activates both astrocyte and microglial states leading to the secretion of large amounts of cytokines and chemokines [13, 14]. In primary mesencephalic neuron-glia cultures from mice and rats, aggregated human α-syn-induced microglial activation led to increased concentrations of reactive oxygen species (ROS), anion superoxide ($O_2^{\cdot-}$), and cyclooxygenase-2-derived prostaglandin E2 with ensuing enhanced DA neurotoxicity [15].

Systemic mitochondrial NADH dehydrogenase (complex I) inhibition in cells or rats by rotenone also promotes α-syn accumulation and aggregation, mitochondrial dysfunction, oxidative damage, and proteasomal dysfunction [16–19]. Moreover, rotenone triggers an inflammatory response and causes DA neuron death [15, 18, 20, 21].

In the present study, we have investigated in detail whether exogenous administration of PFFs can reproduce some of the key pathological features of PD in rat ventral midbrain neuron cultures, including mitochondrial dysfunction and selective DA neuron loss. Experiments were carried out after 14 days incubation (19 DIV), when PFFs generated LB-like proteinaceous insoluble assemblies that can initiate a series of deleterious events leading to overt selective DA cell death. Interestingly, co-treatment with rotenone heightened PFFs-induced toxic effects, resulting in an additive action. Our study also shed light on the molecular mechanisms responsible of PFFs pathogenicity; we provide the first evidence for a direct association between the noxious effects of PFFs and the excessive generation of nitric oxide ($NO^{\cdot}$) as a consequence of upregulated inducible nitric oxide synthase (iNOS) expression levels.

Fig. 1 Exogenous α-syn fibrils mediate α-syn aggregation in dopamine neurons. **a** Neurons were fixed and treated with or without 1% Triton X-100 at 19 DIV. Confocal image acquisition was performed at 100× and zoomed in 3× for TH^+ (*blue*), MAP2 (*gray*), total α-syn (*green*), and α-syn pSer129 (*red*). In PBS-treated neurons, puncta α-syn was mainly located at the presynaptic nerve terminals (**a2**) and was Triton-100 soluble (**a12**). However, α-syn was accumulated in the somata of DA neurons following PFFs administration, leading to the formation of LB-like pathologic inclusions (**a7**) which were Triton X-100 insoluble (**a17**). Treatment with PFFs significantly enhanced the expression levels of pathologic α-syn pSer129 compared to PBS-treated neurons (**a3** vs. **a8**) which remained insoluble (**a18**). *Scale bar* 10 μm. **b** Representative WB from cell lysates. Treatment with 2 and 5 μg/mL PFFs for 14 days caused an increase in monomeric α-syn immunoreactivity and higher molecular weight species of α-syn. Each experimental condition was run in triplicate

Results

Alpha-synuclein fibrils elicit protein accumulation and aggregation in dopamine neurons

Preformed PFFs seed the aggregation and fibrillation of endogenous α-syn in cultured primary hippocampal neurons derived from C57Bl/6 mice [7]. We sought to investigate whether these α-syn expression patterns can be replicated in cultured rat ventral midbrain neurons. Cell cultures were exposed to 2 μg/mL PFFs at 5 DIV and immunolabeled using antibodies against total α-syn and α-syn pSer129 after 14 days incubation (Fig. 1a). Laser scanning confocal images revealed that, in non-treated (PBS) neurons, α-syn is predominantly localized at presynaptic nerve terminals and, to a lesser extent, axons (Fig. 1a2). However, accumulated α-syn was detected in the perikaryon of DA neurons following PFFs addition (Fig. 1a7). Presynaptic endogenous α-syn from PBS-treated neurons was considerably soluble in 1% Triton X-100 (Fig. 1a12), while addition of PFFs produced detergent-

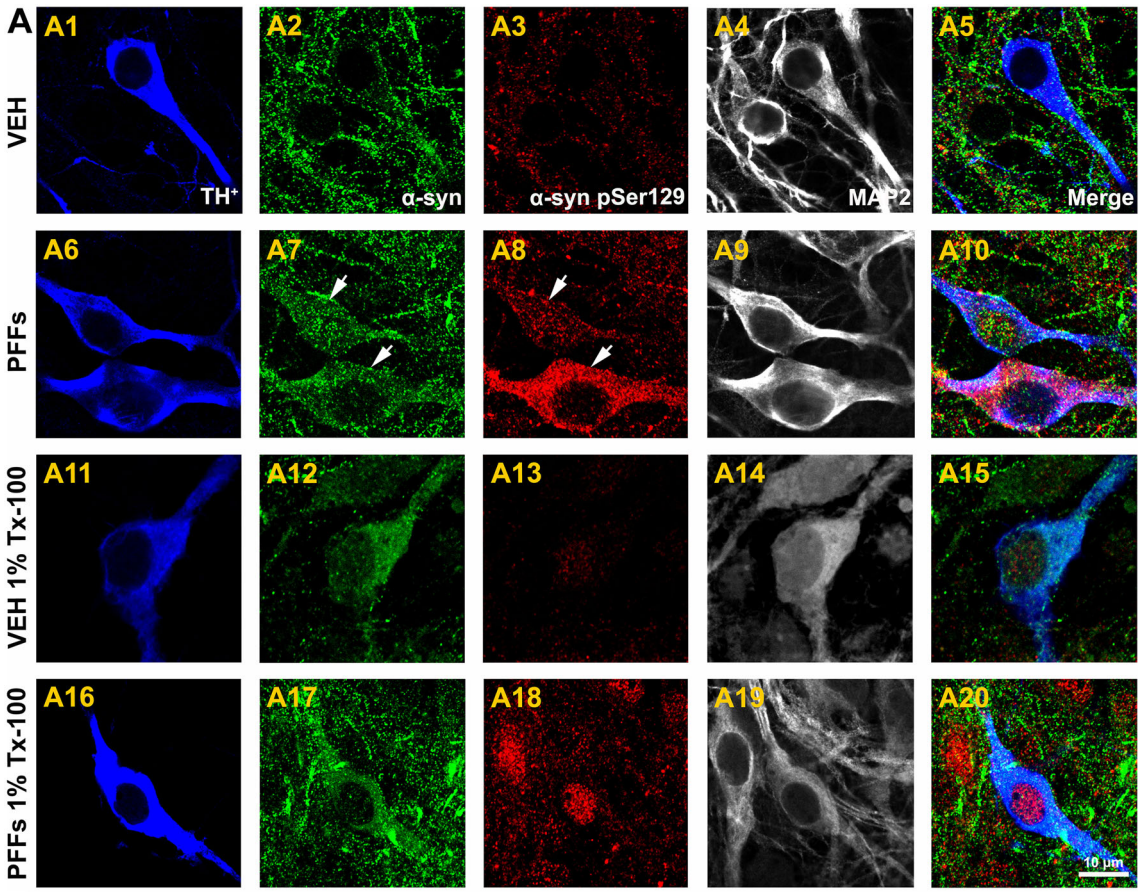
A
VEH
PFFs
VEH 1% Tx-100
PFFs 1% Tx-100
A1
A2
A3
A4
A5
A6
A7
A8
A9
A10
A11
A12
A13
A14
A15
A16
A17
A18
A19
A20
TH+
α-syn
α-syn pSer129
MAP2
Merge
10 µm

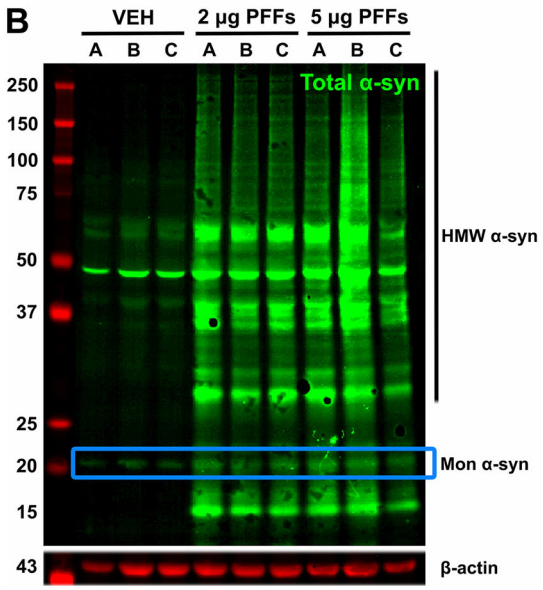
B
VEH
2 µg PFFs
5 µg PFFs
A B C A B C A B C
Total α-syn
250
150
100
75
50
37
25
20
15
43
HMW α-syn
Mon α-syn
β-actin

insoluble α-syn selectively in DA neurons (Fig. 1a17). α-Syn can undergo post-translational modifications in the brain of subjects with PD, including phosphorylation at residue Ser129 [1, 2]. Untreated cells displayed a lack of α-syn pSer129 (Fig. 1a3) but its immunoreactivity was widely enhanced upon PFFs administration (Fig. 1a8) which remained insoluble in 1% Triton X-100 (Fig. 1a18).

Representative confocal images illustrated that cytoplasmic inclusions containing α-syn pSer129 were primarily present in DA neurons compared to astrocytes (Fig. S1). In addition, we surmised that α-syn assembled into high-molecular weight species. Western blot analysis of cell lysates displayed a single band at ~20 kDa corresponding to monomeric α-syn and a smaller band at ~15 kDa consistent with a truncation product of PFFs (Fig. 1b). Antibodies used against α-syn pSer129 did not detect any band in the 2% SDS-extractable fraction likely because of the low percentage of DA neurons in these cultures (~5%; data not shown).

Formation of aggregates is time-dependent

Given the appearance of α-syn multimers and aggregates increase in a time-dependent fashion in mouse brain and cultured mouse hippocampal neurons [7, 22, 23], we examined whether PFFs caused progressive α-syn accumulation in rat DA neuron cultures (Fig. 2). Small α-syn pSer129-positive puncta along neurites were observed 4 days after PFFs addition (Fig. 2a3). By 7 days post PFFs exposure, enhanced levels of α-syn pSer129 were mainly located at the level of axons and presynaptic nerve terminals, though slight α-syn inclusions were detected in the perikarya of some DA neurons (Fig. 2a8). Following fourteen days of treatment with PFFs, LB-like assemblies were seen in axons although they were particularly prominent in the neuronal soma of DA cells (and the nuclei of some DA-containing neurons) (Fig. 2a13). An age-related anomalous increase in α-syn protein levels in the SN of humans and rhesus monkeys and mature mice-cultured hippocampal neurons [7, 24] have been reported. Based on these findings, we investigated whether addition of PFFs to mature neurons would affect α-syn pools, eventually resulting in an increased aggregation rate. When cultures were supplemented with an identical concentration of PFFs at 10 DIV, DA neurons were sparsely immunoreactive to α-syn pSer129 following 2 days of treatment (Fig. 2b3). Enhanced neuritic and soma levels of α-syn pSer129 were found 4 days after PFFs addition (Fig. 2b8). Nine days of treatment with PFFs revealed a marked accumulation of α-syn in the somata and nuclei of DA neurons (Fig. 2b13). Besides, there was a progressive increase in the intensity of total α-syn staining with the time, regardless if PFFs were added at 5 (Fig. 2a2, a7, a12) or 10 (Fig. 2b2, b7, b12) DIV.

Synaptic pathology is linked to alpha-synuclein aggregation

Brain functional imaging methods revealed a decrease of presynaptic structures in dementia with Lewy bodies (DLB) and PD [25]. We therefore assessed whether PFFs may modulate the expression of several synaptic proteins at 19 DIV, when neurons have well-established synaptic network (Fig. 3). Qualitative analysis showed that PFFs induced significant loss of cysteine string protein alpha (CSP-α) and synaptosomal-associated protein 25 (SNAP-25) immunofluorescence in DA neurons, either alone or in combination with rotenone. Assessment of synaptic vesicle fluorescence intensity demonstrated that PFFs caused a substantial decrement of CSP-α (Fig. 3e; 2631 ± 104 vs. 2075 ± 60, $p < 0.01$) and SNAP-25 (Fig. 3g; 2216 ± 96 vs. 1546 ± 60, $p < 0.01$) immunoreactivity in DA neurons. Rotenone evoked severe downregulation of synaptic protein expression relative to vehicle group (Fig. 3e; 2631 ± 104 vs. 1189 ± 15 CSP-α, $p < 0.001$ and Fig. 3g; 2216 ± 96 vs. 243 ± 98 SNAP-25, $p < 0.001$). The effect was even greater when rotenone was administered alongside with PFFs. A striking observation was that non-DA neurons were resistant to PFFs-induced deleterious effects (Fig. 3f, h), suggesting a selective effect on DA neurons.

Likewise, the expression levels of the SNARE protein VAMP2 (vesicle-associated membrane protein 2 or synaptobrevin 2) were abrogated following PFFs intoxication, either alone (Fig. S2 A2 and B2; 2620 ± 82 vs. 2203 ± 49, $p < 0.001$) or together with rotenone (Fig. S2 C2 and D2; 1699 ± 25 vs. 1290 ± 27, $p < 0.001$). Contrarily, PFFs did not alter synaptophysin expression (Fig. S2 A3–D3).

Alpha-synuclein fibril treatment results in axonal transport deficits

Axonal transport is mediated by the motor proteins kinesin and dynein. Fast anterograde transport is responsible for carrying axolemmal precursors, mitochondria, and synaptic vesicles to the axon. Defective axonal transport is a common factor in several neurodegenerative diseases, including PD [24]. To determine whether axonal transport abnormalities can be ascribed to PFFs toxicity, cells were labeled with TH, MAP2, KLC1, and KHC markers and subjected to confocal microscopy analysis (Fig. 4). PFFs addition reduced KHC expression in DA neurons relative to PBS-treated cells (Fig. 4g; 2823 ± 79 vs. 2229 ± 87, $p < 0.001$). Likewise, a strong decline in KHC fluorescence was detected following rotenone exposure (Fig. 4g; 2823 ± 79 vs. 1883 ± 21, $p < 0.0001$). Important differences were seen in the levels of KHC between rotenone-stimulated cells treated with PFFs compared to rotenone-treated cells that did not receive PFFs (Fig. 4g; 1346 ± 89

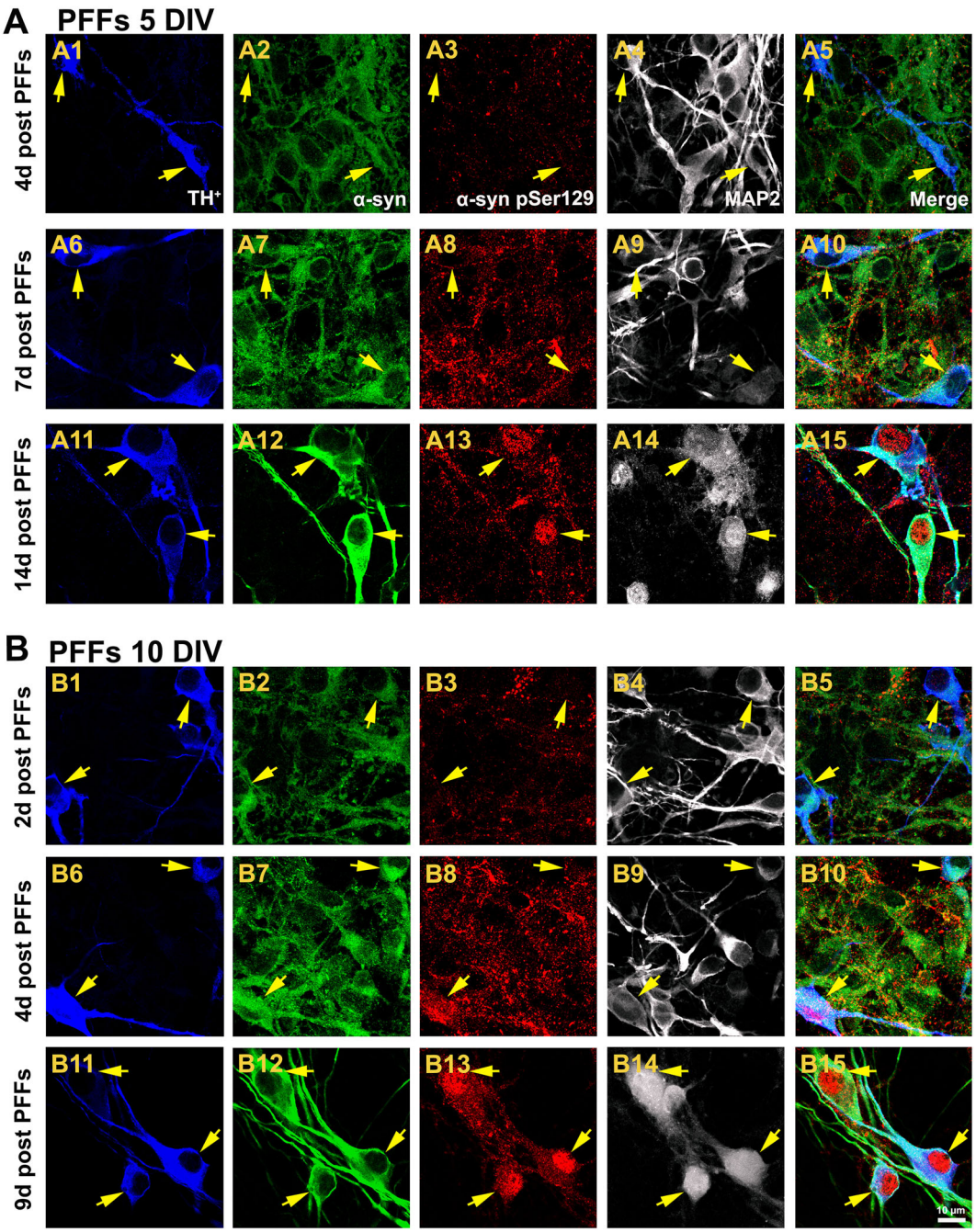

Fig. 2 Aggregate formation is time-dependent. **a** Neuronal cultures were exposed to PFFs at 5 DIV and qualitative assessment was carried out at different time points. Confocal laser scanning micrographs at 200× magnification depicted a weak α-syn pSer129 staining in the presynaptic puncta after 4 days PFFs administration (**a3**). At 7 days of treatment, α-syn pSer129 immunoreactivity was predominantly observed at the presynaptic terminals and axons but also LN and small LB were detected (**a8**). By 14 days post PFFs exposure, upregulated expression of α-syn pSer129 was more intense, and LB-like assemblies were found in the perikarya (and some nuclei) of DA neurons (**a13**). **b** An identical concentration of PFFs was tested in mature neurons at 10 DIV. Cells displayed a faint α-syn pSer129 staining following 2 days of PFFs treatment (**b3**). α-Syn accumulation was observed in both LN and LB four days post PFFs addition (**b8**). By 9 days of PFFs exposure, pathological α-syn pSer129 was particularly found within the nucleus and soma of DA neurons (**b13**). Overall α-syn immunoreactivity (*green*) was increased in a time-dependent manner regardless if PFFs were added at 5 or 10 DIV. *Scale bar* 10 µm

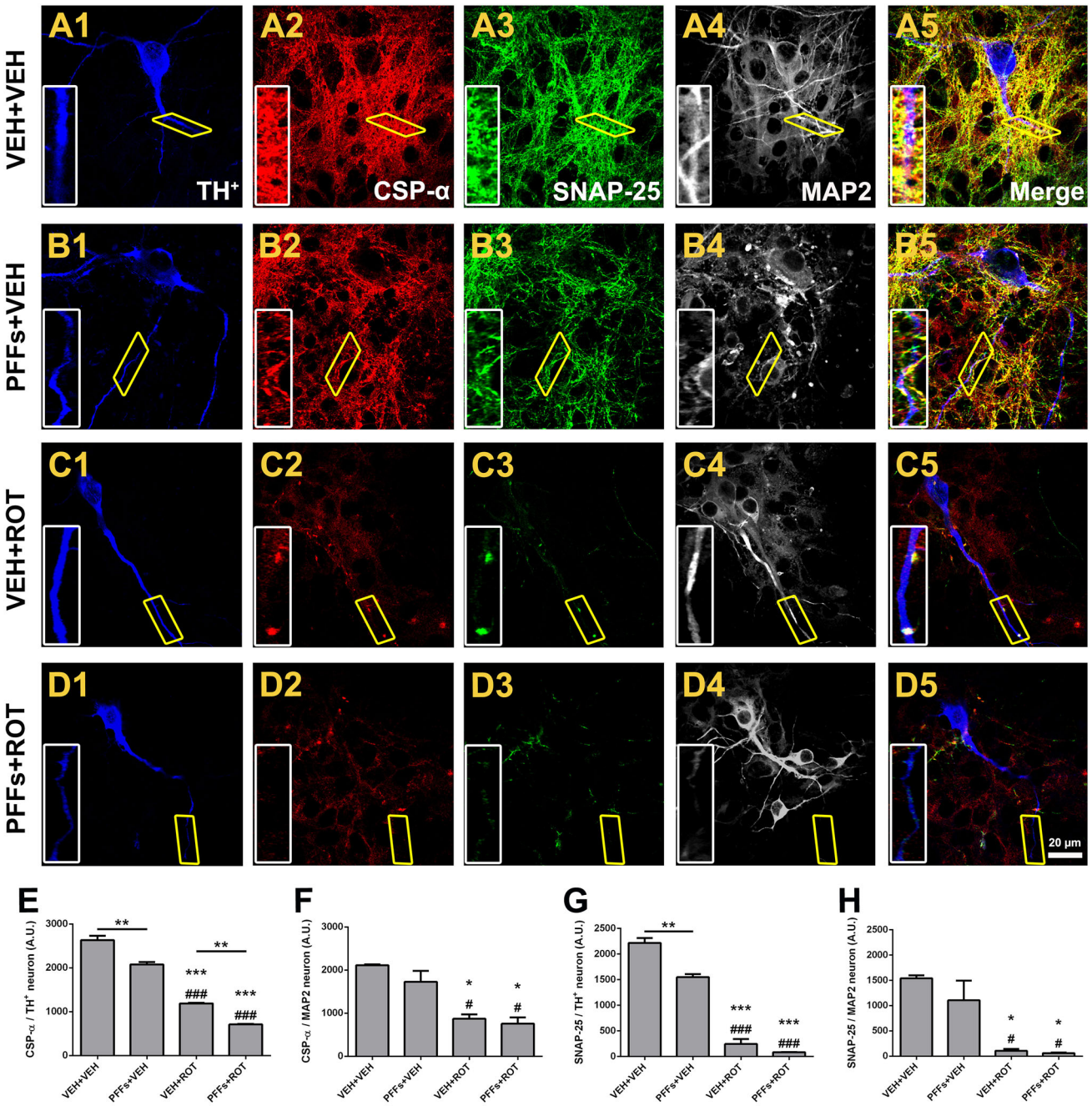

Fig. 3 Neuronal α-syn fibril accumulation modulates synaptic protein expression in dopamine neurons. **a–d** Representative scans from immunocytochemical preparations obtained at 100× at 19 DIV. A progressive decline in synaptic protein expression was noticed after treatment with PFFs (**b2**, **b3**), rotenone (**c2**, **c3**), and PFFs plus rotenone (**d2**, **d3**) relative to vehicle-treated neurons. PFFs exhibited a specific deleterious effect on DA neurons (TH^+, *blue*) but found no difference on non-DA neurons (MAP2, *gray*). *Insets* correspond to high magnification images. **e** Quantification of CSP-α fluorescent intensity in DA neurons. **f** Expression levels of CSP-α in non-DA neurons. SNAP-25 immunofluorescence rate in DA (**g**) and non-DA neurons (**h**). The average of two independent experiments was obtained for synaptic protein evaluation, performed in $n = 3$ wells per condition and experiment. Data are expressed as mean ± SEM and analyzed using one-way ANOVA followed by Newman–Keuls multiple comparisons test. $^{***}p < 0.001$, $^{**}p < 0.01$, and $^{*}p < 0.05$ compared to VEH + VEH. $^{\#\#\#}p < 0.001$ and $^{\#}p < 0.05$ vs. PFFs + VEH. $^{**}p < 0.01$ relative to VEH + ROT. *Scale bar* 20 µm

vs. 1883 ± 21, $p < 0.001$). Strikingly, PFFs had a slight effect on non-DA neurons ($p < 0.05$) and no additive effect was observed when fibrils were combined alongside with rotenone (Fig. 4h). The immunoreactivity of KLC1 remained unchanged after PFFs or rotenone incubation in DA and non-DA neurons (Fig. 4e, f).

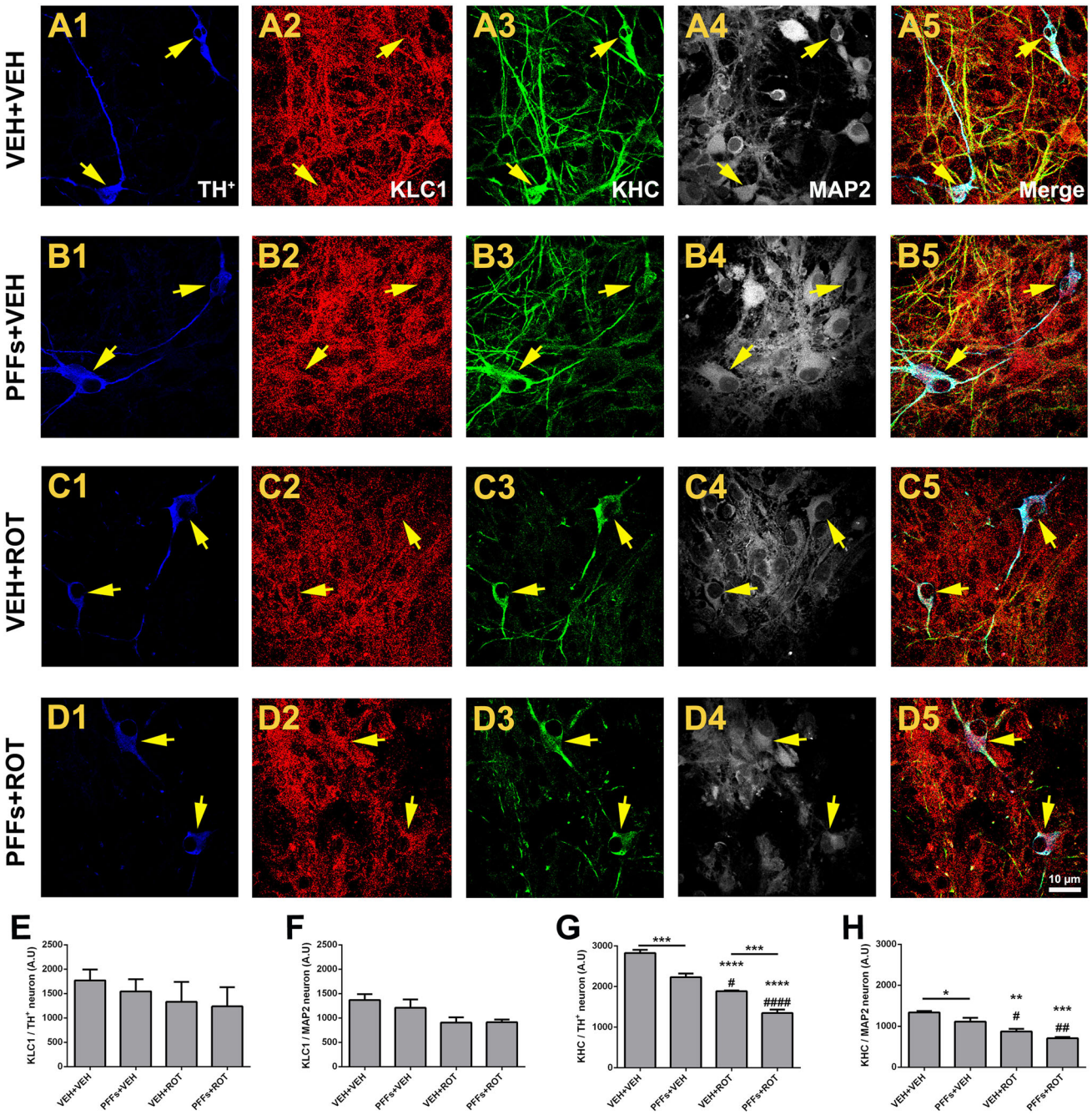

Fig. 4 Seeded fibrils induce axonal transport-related protein deficiencies in dopaminergic neurons. Series of high-resolution confocal microscopy images of DA neuron cultures at 100× depicting KLC1 (*red*) and KHC (*green*) expression levels. Although no appreciable changes were noticed in KLC1 fluorescence intensity, the expression of KHC was steeply downregulated in DA neurons following PFFs exposure (**a**–**d**). Bar graph comparing the levels of KLC1 in DA (**e**) and non-DA (**f**) neurons. **g** Histogram depicting KHC immunofluorescence DA neurons. **h** Quantitative analysis of KHC levels in non-DA neurons. Data are mean ± SEM representative of the average of ~20–30 TH^+ and 500–700 MAP2 neurons from three separate experiments done in triplicate for each culture condition. $^{****}p < 0.0001$, $^{***}p < 0.001$, and $^{**}p < 0.01$ vs. VEH + VEH. $^{\#\#\#\#}p < 0.0001$, $^{\#\#}p < 0.01$, and $^{\#}p < 0.05$ compared to PFFs + VEH. $^{***}p < 0.001$ compared to VEH + ROT (one-way ANOVA followed by Newman–Keuls multiple comparisons test). *Scale bar* 10 µm

Selective accumulation of H2AX Ser139 in DA neurons after alpha-synuclein fibril administration

Accumulation of DNA lesions leads to progressive decline of mitochondrial function and is considered to be a prime factor in aging and neurodegeneration. Histone H2AX phosphorylation at Ser139 (γ-H2AX) has been used as an indirect marker of DNA double-strand breaks (DSB) [26]. Thus, neurons were labeled with γ-H2AX, and the effect of PFFs and/or rotenone was tested (Fig. 5). Neurons incubated with PBS depicted a faint γ-H2AX signal in (Fig. 5a2). A notable enhancement of γ-H2AX immunoreactivity was found following PFFs addition (Fig. 5b2, e; 1559 ± 67 vs. 1011 ± 44, $p < 0.001$). Rotenone (Fig. 5c2, e; 2029 ± 57 vs. 1011 ± 44, $p < 0.0001$) and particularly PFFs + ROT (Fig. 5d2, e; 2697 ± 96 vs. 2029 ± 57, $p < 0.001$) groups presented substantially elevated levels of γ-H2AX in remaining DA neurons. Interestingly, no considerable differences were detected for H2AX Ser 139 expression in non-DA neurons except a slight increase in the PFFs + ROT group relative to VEH + ROT-treated cells (Fig. 5f).

Alpha-synuclein fibrils compromise DA neuron survival in a dose- and time-dependent manner

Because PFFs induce a variety of different deleterious events in DA neurons, we speculated that α-syn fibrils per se may jeopardize DA neuron survival. To test this hypothesis, neuronal cultures were incubated with serial dilutions of PFFs of over a time-course. Quantitative near-infrared analysis revealed that, at 9 DIV, TH content was unaffected among all groups (Fig. 6a). On 12 DIV, TH optical density still remained invariable except for the largest dose of PFFs (20 μg/mL PFFs) that considerably dampened TH immunoreactivity ($p < 0.0001$). Following 14 days of treatment, TH protein levels were diminished by PFFs in a concentration-sensitive manner (Fig. 6a, c). Long-term treatment with the highest dose of PFFs caused non-selective neuron toxicity, as indicated by reduced MAP2 expression (Fig. 6b, c). Unbiased cell counting established that PFFs did not cause any deleterious effect after 4 or 7 days post-administration (Fig. 6d–g). Nevertheless, PFFs treatment for two weeks resulted in a significant depletion of DA-producing neurons in comparison to cells that received vehicle treatment (Fig. 6h; 1070 ± 64 vs. 1330 ± 79, $p < 0.05$). As expected, neurons exposed to rotenone displayed a dramatic decline in the number of DA neurons (Fig. 6h; 680 ± 32 vs. 1330 ± 79, $p < 0.0001$). Addition of PFFs and rotenone led to considerable decrease in DA population content compared to non-treated cells (Fig. 6h; 488 ± 60 vs. 1330 ± 79, $p < 0.0001$) and rotenone-alone group (Fig. 6h; 488 ± 60 vs. 680 ± 32, $p < 0.05$). The number of non-DA neurons remained unaltered across PFFs treatment (Fig. 6i). Neuronal counts were confirmed by WB analysis (Fig. S3).

Pathological alpha-synuclein fibrils undermine mitochondrial function

Considerable evidence emerging from recent studies suggests that α-syn exhibits preferential binding affinity for mitochondria compared to other organelles and its mitochondrial import is ATP- and membrane potential-dependent [8, 27]. We therefore investigated whether PFFs provoked mitochondrial dysfunction (Fig. 7). PFFs-treated cells had similar basal oxygen consumption rates relative to PBS-treated neurons (Fig. 7a1); however, exposure to PFFs resulted in a diminished spare respiratory capacity (Fig. 7a2; 30 ± 4 vs. 45 ± 2 pmol/min, $p < 0.01$) and enhanced proton leak relative to PBS-treated cells (Fig. 7a3; 10.9 ± 1.5 vs. 7.8 ± 0.5 pmol/min, $p < 0.05$).

Mitochondrial fusion and fission play a primary role in controlling mitochondrial shape, movement, and function. It has been reported that α-syn impairs mitochondrial dynamics in cell and animal models of PD [28, 29]. We studied whether PFFs could alter the expression of mitochondrial fusion and fission-linked proteins (Fig. 7b). Analysis revealed that Opa1 expression—a key mediator of fusion of the inner mitochondrial membrane—was depleted in DA neurons following PFFs administration (Fig. 7b21; 3147 ± 37 vs. 2572 ± 73, $p < 0.01$). Rotenone exposure provoked a higher attenuation of Opa1 immunoreactivity (Fig. 7b21; 3147 ± 37 vs. 1954 ± 54, $p < 0.0001$). The combination of PFFs and rotenone showed an additive decrease in Opa1 expression levels in comparison to rotenone alone-treated neurons (Fig. 7b21; 1954 ± 54 vs. 1458 ± 31, $p < 0.001$). In regards to non-DA neurons, Opa1 immunofluorescence was slightly dampened in vehicle-treated cells that receive PFFs vs. neurons that did not receive PFFs, whereas no substantial variations were noticed among the VEH + ROT and PFFs + ROT groups (Fig. 7b22). On the other hand, the levels of the fission protein Drp1 remained unchanged in DA neurons (Fig. 7b23) but were slightly reduced in MAP2 neurons (Fig. 7b24).

Live-cell imaging analysis was performed to determine whether PFFs were able to modulate mitochondrial ROS production. MitoSOX Red signal—that measures the generation of $O_2^{\cdot-}$—was monitored and recorded over a ~30 min time frame. The signal was normalized with baseline fluorescence detected prior to PFFs or rotenone application. Individual traces revealed that PFFs exposure considerably elevated the rate of ROS within mitochondria (Fig. S4 B). Rotenone administration elicited a sharp increase in MitoSOX levels (Fig. S4 C and E). In addition,

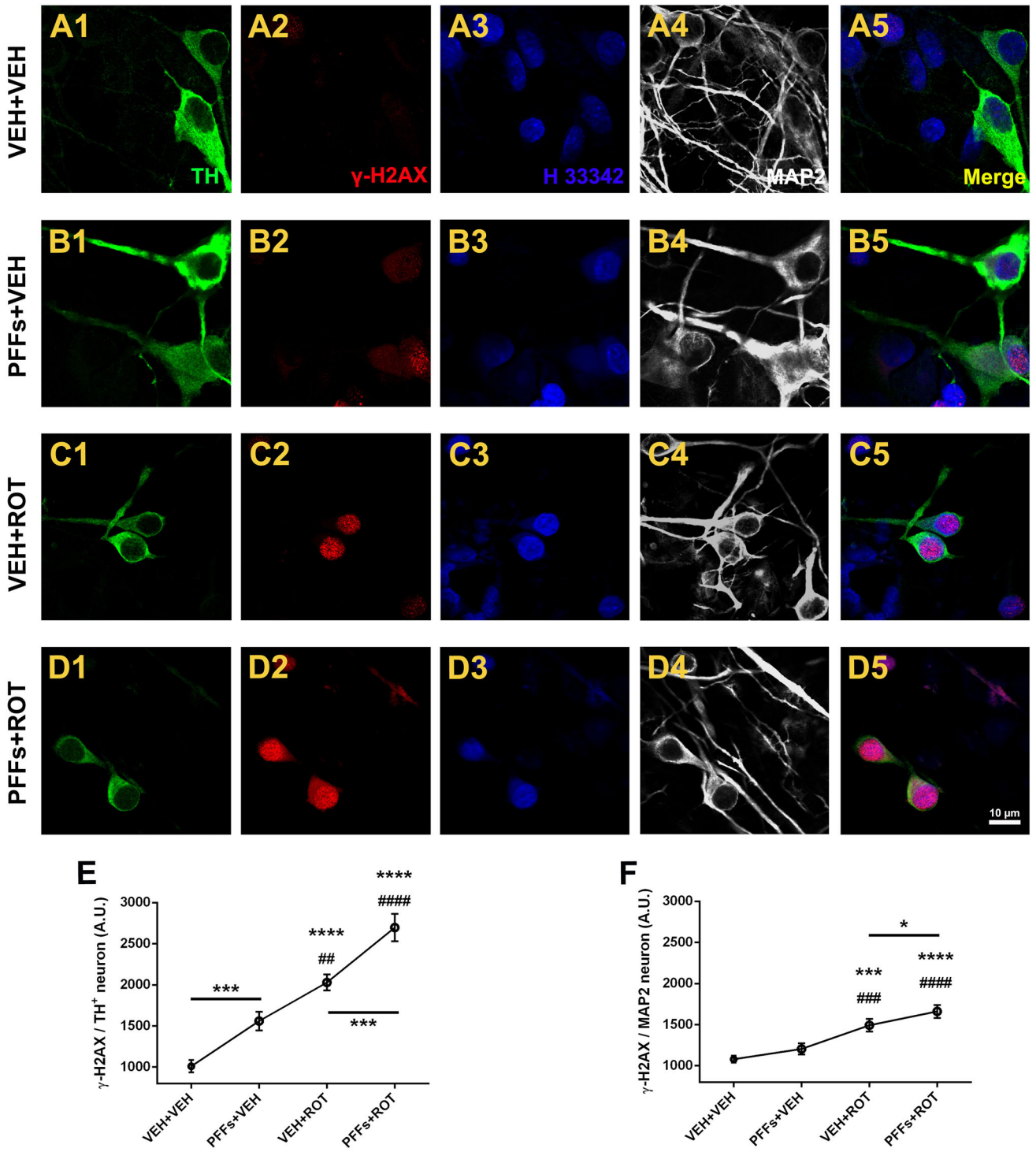

Fig. 5 α-Syn fibrils elicit selective γ-H2AX immunoreactivity in dopamine-immunoreactive neurons. **a–d** Neurons were labeled with γ-H2AX, TH^+, and MAP2 antibodies and H 33342. Increased immunoreactivity for γ-H2AX within TH^+ neurons was detected following PFFs administration (**a2** vs. **b2**, 55%). Rotenone exposure also exacerbated the levels of γ-H2AX (**c2**, 100%). Combined treatment of PFFs and rotenone led to higher γ-H2AX expression (**d2**, 170%). **e** Quantification of endogenous γ-H2AX levels in DA neurons. **f** Barogram showing fluorescence intensity values of γ-H2AX in non-DA neurons. Data from three independent experiments in triplicate were pooled and presented as the average mean fluorescence intensity ± SEM. Around 40–50 TH^+ and 800–1000 MAP2 neurons were examined. $^{****}p < 0.0001$ and $^{***}p < 0.001$ relative to VEH + VEH. $^{\#\#\#\#}p < 0.0001$, $^{\#\#\#}p < 0.001$, and $^{\#\#}p < 0.01$ compared to PFFs + VEH. $^{***}p < 0.001$ and $^{*}p < 0.05$ compared to VEH + ROT (one-way ANOVA followed by Newman–Keuls multiple comparisons test). *Scale bar* 10 µm

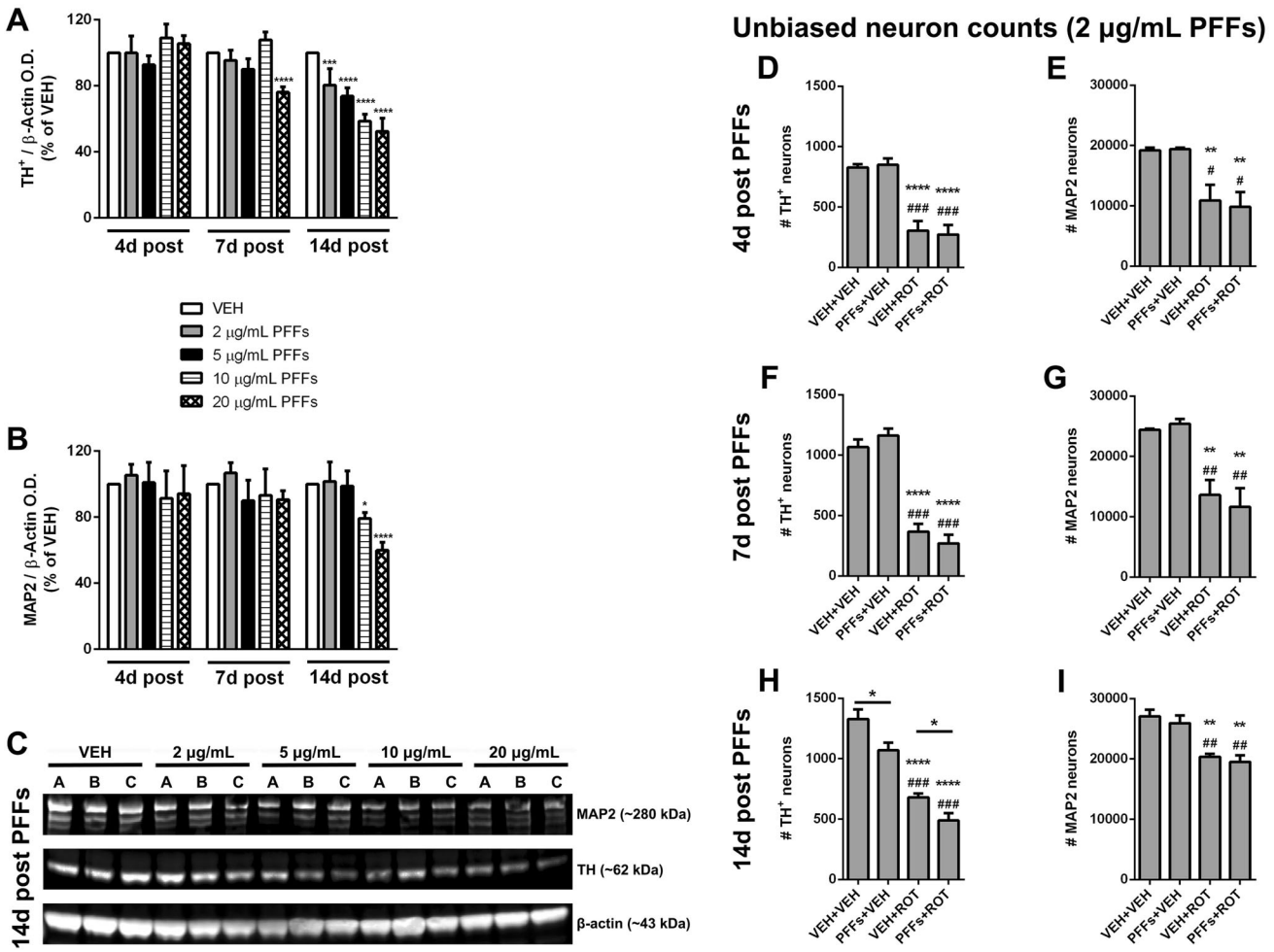

Fig. 6 α-Syn fibrils lead to specific dopaminergic neuronal death. **a**–**c** Cells were treated with different concentrations of PFFs and harvested at different time points. **a** Quantitative near-infrared immunoblotting was employed to measure TH^+ immunoreactivity. PFFs did not exert any noxious effect following 4 or 7 days exposure, except the highest dose of PFFs (20 μg/mL). By 14 days post PFFs incubation, all doses tested diminished TH^+ expression dose-dependently. **b** PFFs did not produce adverse effects on non-DA neurons at low concentration; nevertheless, after 14 days treatment, high doses of PFFs were found to significantly decrease MAP2 densitometric values. **c** Representative immunoblot probed with anti-TH and -MAP2 at 19 DIV. β-Actin was used for loading control normalization. Results were normalized to percentage neuron survival of vehicle control cells. Histograms showing unbiased neuron counts in DA (**d**, **f**, **h**) and non-DA neurons (**e**, **g**, **i**). Data from four independent cultures in triplicate were combined to determine mean ± SEM. $^{****}p < 0.0001$, $^{***}p < 0.001$, $^{**}p < 0.01$, and $^{*}p < 0.05$ relative to VEH + VEH. $^{###}p < 0.001$, $^{##}p < 0.01$, and $^{#}p < 0.05$ vs. PFFs + VEH. $^{*}p < 0.05$ compared to VEH + ROT (one-way ANOVA followed by Newman–Keuls multiple comparisons test)

combined treatment with PFFs, and rotenone exacerbated $O_2^{\cdot-}$ production in a concentration-dependent manner (Fig. S4 D and F). Pooled data exhibited a ~5-fold increase in MitoSOX levels after PFFs treatment, which were higher in the PFFs + ROT group (Fig. 7c). Furthermore, no alterations in mitochondrial mass were noticed after PFFs addition, either in DA or non-DA neurons (Fig. S5).

Involvement of nitrosative stress in alpha-synuclein fibril-induced neurotoxicity

Oxidation of proteins has been proposed to be the prevailing modification caused by RNS generated from $NO^{\cdot}$. Protein tyrosine nitration is a characteristic feature of α-synucleinopathies, including PD. We examined whether PFFs increased the rate of nitrotyrosine (3-NT) expression (Fig. 8). DA neurons were particularly susceptible to PFFs-induced protein nitration compared to vehicle treatment group (Fig. 8b2 vs. a2; 1933 ± 53 vs. 1624 ± 51, $p < 0.05$). The degree of proteins that underwent 3-NT modification was higher after rotenone exposure relative to both VEH + VEH and PFFs + VEH groups (Fig. 8c2 vs. a2 and b2; 2434 ± 55 vs. 1624 ± 51; and 1933 ± 53, $p < 0.001$ and $p < 0.01$, respectively). Addition of rotenone alongside with PFFs upregulated 3-NT immunoreactivity compared to rotenone alone-treated cells (Fig. 8d2 vs. c2; 2877 ± 120 vs. 2434 ± 55, $p < 0.01$). Overall, 3-NT immunostaining remained

comparatively unchanged within MAP2 neuronal population (Fig. 8f).

Converging lines of evidence indicates that mitochondria constitute a primary locus for protein tyrosine nitration. Complexes I and III are the main site of $O_2^{\cdot-}$ release and may react with $NO^{\cdot}$ to form $ONOO^-$, which causes irreversible injury to mitochondria and raises the yield of 3-NT levels. However, no change was observed in the Pearson's correlation coefficient values between 3-NT and TOM20 in DA neurons (Fig. S6), indicating that enhanced PFFs-mediated 3-NT synthesis occurs predominantly in the cytosol.

Inflammatory response to alpha-synuclein fibril exposure

Inflammation may play a prominent role in α-syn fibrillation and constitutes a key pathogenic event in neurodegenerative disorders. $NO^{\cdot}$ is synthesized from L-arginine in a reaction catalyzed by the NOS enzyme, which exists in both constitutive and inducible isoforms (iNOS). $NO^{\cdot}$ can be further generated by the mitochondrial NOS which is located in the inner membrane and appears to exist as constitutive and inducible forms [11, 30]. We assessed quantitative modifications in inflammatory molecule expression profiles (Fig. 9). DA neurons exposed to PFFs displayed a marked increase in iNOS protein levels compared to vehicle-treated neurons (Fig. 9a1, a2 and Fig. 9a3, a4; 242 ± 17 vs. 436 ± 15, $p < 0.001$). Rotenone exposure elevated iNOS immunoreactivity (Fig. 9a1, a2 and Fig. 9a5, a6; 242 ± 17 vs. 707 ± 22, $p < 0.0001$). Addition of PFFs to rotenone-treated neurons enhanced the rate of iNOS in comparison with the rotenone-alone group (Fig. 9a5, a6 and Fig. 9a7, a8; 707 ± 22 vs. 910 ± 29, $p < 0.001$). A similar pattern was found in non-DA neurons, though the total PFFs-mediated iNOS expression levels were lower relative to those generated in DA neurons (Fig. 9a9 vs. a10; $p < 0.05$).

To further characterize the role of other proinflammatory mediators, whole-cell lysates were immunoblotted with NF-κB subunit p65, TNF-α (tumor necrosis factor α), COX-2, and IL-1β antibodies (Fig. 9b). Data analysis demonstrated that NF-κB p65 levels were increased in the PFFs + ROT group (Fig. 9b2, $p < 0.05$); although did not reach statistical significance, there was a trend toward higher NF-κB p65 expression in PFFs + VEH-stimulated cells. PFFs or rotenone administration evoked an elevated expression of TNF-α levels (Fig. 9b3, $p < 0.01$ and $p < 0.001$, respectively). Besides, PFFs + ROT treatment significantly enhanced TNF-α content relative to the VEH + ROT group (Fig. 9b3, $p < 0.01$). In contrast, addition of PFFs to neuron cultures did modify neither COX-2 nor IL-1β protein levels (Fig. 9b4–b6). Furthermore, we could not detect any substantial variation in microglial activation—including average size, number of cells, and overall area covered—following PFFs intoxication, monitored by Iba1 expression (Fig. S7).

Downregulation of iNOS dampens nitrotyrosine protein expression and protects against overt dopamine neuron demise

We aimed to elucidate a mechanism underlying PFFs-induced selective DA pathogenicity. Based upon our observations that 3-NT levels were specifically enhanced in DA neurons after PFFs administration, we can speculate that $NO^{\cdot}$ may play a critical role in mediating PFFs neurotoxicity, supporting the premise that oxidative stress contributes to the pathogenesis of α-synucleinopathies (and PD). Here, we tested whether selective inhibition of iNOS by the 1400 W compound might halt or drop 3-NT synthesis after PFFs exposure (Fig. 10). Neuron cultures were therefore incubated with or without 10 μM 1400 W for 4 h before PFFs addition at 5 DIV. Nineteen-day-old cultures were subjected to immunocytochemistry using anti-iNOS and -3-NT antibodies. Pretreatment with 1400 W had no effect in iNOS basal immunoreactivity in the vehicle group but it was extraordinarily effective toward diminishing iNOS expression levels in DA neurons stimulated with PFFs (Fig. 10q; 431 ± 12 vs. 665 ± 15, $p < 0.0001$). A parallel decrease in 3-NT immunoreactivity was observed upon 1400 W administration in PFFs-treated cells compared to those that did not receive 1400 W (Fig. 10r; 1393 ± 17 vs. 1659 ± 22, $p < 0.0001$).

We further assessed whether blocking iNOS expression prevented against PFFs-induced DA-containing neuron demise. On the 5 DIV, cells were treated as described above and immunostained with TH and MAP2 markers and counterstained with H 33342 (Fig. 11). Quantitative assessment revealed that PFFs treatment elicited a substantial reduction in the number of TH^+ neurons (~30%) in the absence of 1400 W (Fig. 11i; 766 ± 41 vs. 1089 ± 50, $p < 0.0001$), whereas pretreatment with 1400 W nearly provided complete neuroprotection against PFFs-induced selective DA toxicity (Fig. 11i; 1021 ± 57 vs. 766 ± 41, $p < 0.001$). No changes were noticed in the number of MAP2 neurons between groups (Fig. 11j).

Discussion

We present compelling evidence that exposure to PFFs of primary ventral midbrain neurons evoked LB-like intraneuronal inclusions that led to a cascade of deleterious cellular responses with ensuing progressive and selective DA neuron death. Moreover, we found that rotenone

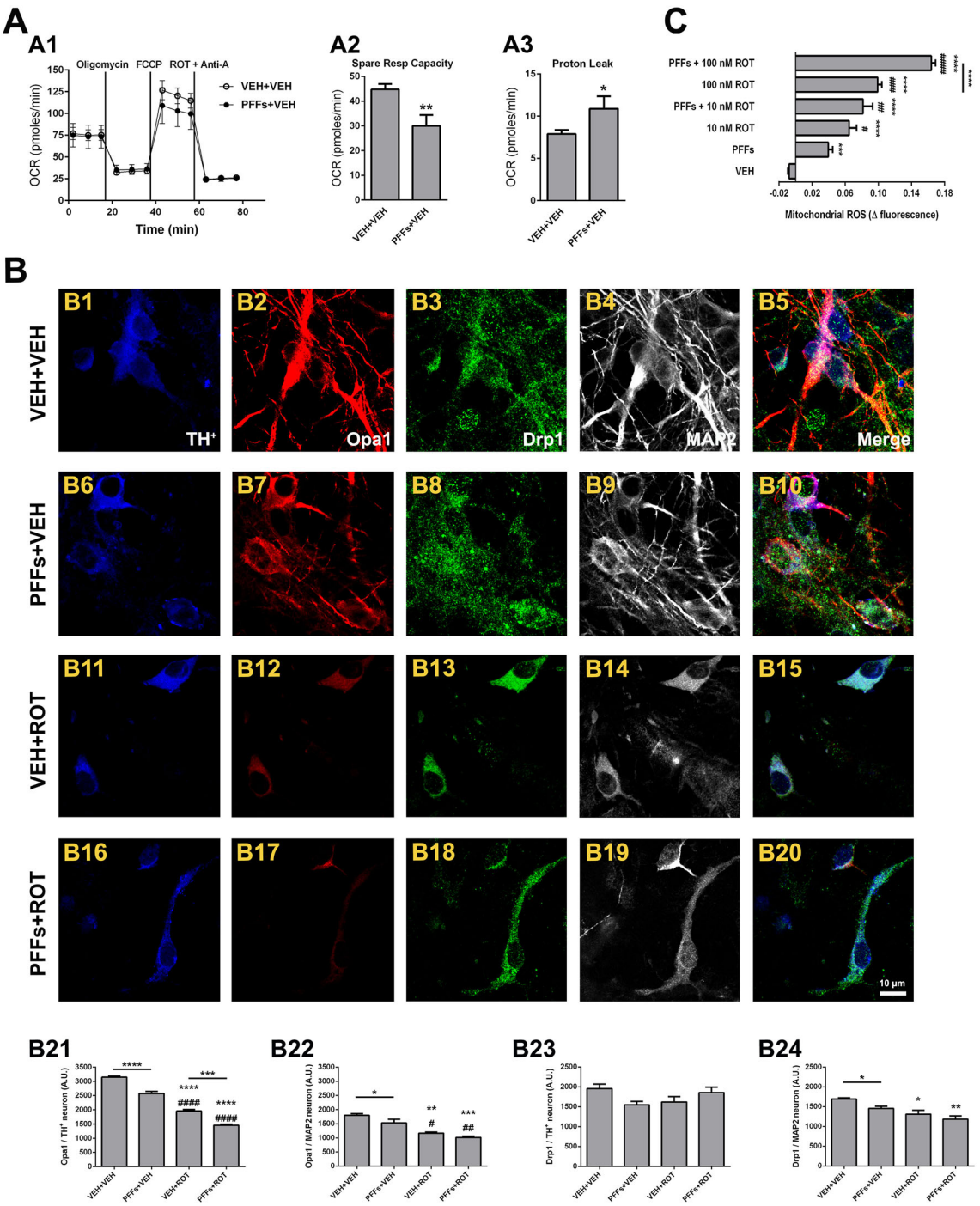
A
A1
Oligomycin FCCP ROT + Anti-A
VEH+VEH
PFFs+VEH
OCR (pmoles/min)
Time (min)
A2
Spare Resp Capacity
OCR (pmoles/min)
VEH+VEH
PFFs+VEH
A3
Proton Leak
OCR (pmoles/min)
VEH+VEH
PFFs+VEH
C
PFFs + 100 nM ROT
100 nM ROT
PFFs + 10 nM ROT
10 nM ROT
PFFs
VEH
Mitochondrial ROS (Δ fluorescence)
B
VEH+VEH
PFFs+VEH
VEH+ROT
PFFs+ROT
B1
TH+
B2
Opa1
B3
Drp1
B4
MAP2
B5
Merge
B6
B7
B8
B9
B10
B11
B12
B13
B14
B15
B16
B17
B18
B19
B20
10 µm
B21
Opa1 / TH+ neuron (A.U.)
VEH+VEH
PFFs+VEH
VEH+ROT
PFFs+ROT
B22
Opa1 / MAP2 neuron (A.U.)
B23
Drp1 / TH+ neuron (A.U.)
B24
Drp1 / MAP2 neuron (A.U.)

◀**Fig. 7** α-Syn fibrils induce mitochondrial dysfunction. PFFs treatment resulted in specific mitochondrial impairments compared to PBS-treated neurons (**a1**), as indicated by lower spare respiratory capacity (**a2**), and increased proton leak (**a3**). Samples were run and analyzed in triplicate and used to calculate the average signal intensity ± SEM. $^{**}p < 0.01$ and $^{*}p < 0.05$ compared to VEH + VEH (unpaired Student *t* test). **b** Series of confocal images acquired at 200× magnification from cells stained with primary antibodies against Opa1 (*red*) and Drp1 (*green*). The bar graphs show a dramatic and progressive reduction of Opa1 levels in PFFs-, rotenone-, and PFFs plus rotenone-treated DA neurons (**b21**) albeit not major changes were observed in non-DA neurons (**b22**). Overall, Drp1 immunoreactivity remained unaltered following PFFs exposure, except a slight decrease in MAP2 neurons (**b23**, **b24**). Values are shown as mean ± SEM and were pooled from three independent datasets performed in triplicate. An average of ~20–25 TH^+ and 550–650 MAP2 neurons were tested. *Scale bar* 10 μm. $^{****}p < 0.0001$, $^{***}p < 0.001$, $^{**}p < 0.01$, and $^{*}p < 0.05$ vs. VEH + VEH. $^{\#\#\#\#}p < 0.0001$, $^{\#\#}p < 0.01$, and $^{\#}p < 0.05$ compared to PFFs + VEH. $^{***}p < 0.001$ compared to VEH + ROT (one-way ANOVA followed by Newman–Keuls multiple comparisons test). **c** Real-time measurement of ROS generation. In the studied time frame (30 min), the increment in fluorescence was linear in the vehicle group and administration of either PFFs or rotenone enhanced the signal. The combination of PFFs and rotenone induced a more robust increment in MitoSOX, resulting in an additive effect. Error bars indicate the mean ± SEM. Measurements were conducted at least 3 times for all conditions from three independent neuron cultures. On an average, ~30–40 neurons per condition were examined. $^{****}p < 0.0001$ and $^{***}p < 0.001$ compared to VEH. $^{\#\#\#\#}p < 0.0001$, $^{\#\#\#}p < 0.001$, $^{\#\#}p < 0.01$, and $^{\#}p < 0.05$ relative to PFFs. $^{****}p < 0.0001$ vs. 100 nM ROT (one-way ANOVA followed by Newman–Keuls multiple comparisons test)

heightened the pathogenic effects of PFFs on DA cells. α-Syn deposits found in brains of subjects diagnosed with LB disorders, including PD, are mainly phosphorylated at residue Ser129 [1, 2]. A time-dependent accumulation and aggregation of α-syn pSer129 was observed in our model. Interestingly, some DA-producing neurons exhibited immunoreactivity for α-syn pSer129 in both cytoplasm and nucleus. In agreement with our outcomes, previous investigations have reported a nuclear immunostaining of α-syn phosphorylated at residue S129 in HEK293 cells, hippocampus and neocortex of mice, and DA cell bodies in the SN of monkeys [31–33]. Our results also revealed that intracellular pools and deposition rate of α-syn became considerably faster in mature neuronal populations, suggestive of a time-dependent process.

α-Syn is predominantly located at the presynaptic termini where it operates as a co-chaperone with CSP-α. It has been proposed that α-syn promotes SNARE-complex formation upon direct binding to SNAP-25 and/or VAMP2, proteins implicated in controlling the release of neurotransmitters through the synaptic vesicle docking and fusion steps [34]. Overexpression of α-syn rescued the neurodegenerative phenotype of mice lacking CSP-α [35]. Synaptic pathology and reduced presynaptic structures related to α-syn aggregation have been observed in PD and DLB human brains and mice hippocampal neuron cultures [7, 25]. We found a selective decreased expression of several presynaptic markers in DA cells, suggesting that pathological α-syn erodes neuronal function and may compromise DA neuron survival.

A leading premise postulates that aggregation of α-syn in LB mediates axonal pathology and leads to progressive brain damage. Galvin and colleagues reported axonal transport impairment in α-syn-immunoreactive neurons in the hippocampal region in postmortem brains of PD and DLB patients [36]. In addition, anterograde protein levels were affected during early stages in SN DA neurons in sporadic PD while retrograde-related proteins were reduced in late stages of the disease [24]. Targeted AAV vector-mediated overexpression of human α-syn into the SN of rats evoked changes in axonal transport-associated proteins in DA neurons bearing α-syn inclusions [24, 37]. Our findings show that PFFs reduced KHC immunoreactivity in DA neurons, thereby suggesting that aggregated α-syn might be the primary culprit of axonal transport deficiency in this experimental paradigm. α-Syn can also contribute to DA neurodegeneration by raising the load of deleterious DNA mutations. A direct correlation between LB pathology and mitochondrial DNA deletions in the SN from postmortem PD subjects has been established [38]. There was an accumulation of DSB in the DNA of A53T mutant α-syn mice through $ONOO^-$-mediated oxidative stress [39]. Our results demonstrated a considerable increase in the DNA DSB marker γ-H2AX.

According to the detrimental phenomena described above, we reasoned that PFFs may render DA neurons more vulnerable to degenerate. It has been proposed that α-syn may negatively modulate TH activity by either direct interaction with the enzyme [9, 40] or decreasing its gene expression [41]. AAV-based gene therapy studies overexpressing wild-type or mutant α-syn into the SN of rat brain induced progressive and selective neurodegeneration in DA neurons [40, 42]. Herein, we determined that PFFs selectively elicited DA neuron loss in a dose- and time-dependent manner. A growing body of evidence suggests that mitochondrial dysfunction and concomitant oxidative stress play a pivotal role in α-syn-induced neurotoxicity, creating a synergistic interrelationship that contributes to the overall complexity of PD. Transgenic mice harboring the A53T α-syn mutation developed LB-like pathologic assemblies and degenerating mitochondria in the brainstem [39]. Misfolded or aggregated α-syn promoted mitochondrial abnormalities and associated oxidative stress in the GT1-7 immortalized cell line [10]. Incubation with amyloid fibrils elevated mitochondrial ROS production in primary neuronal cultures of either the cortex or glia [43]. α-Syn overexpression potentiated mitochondrial ROS

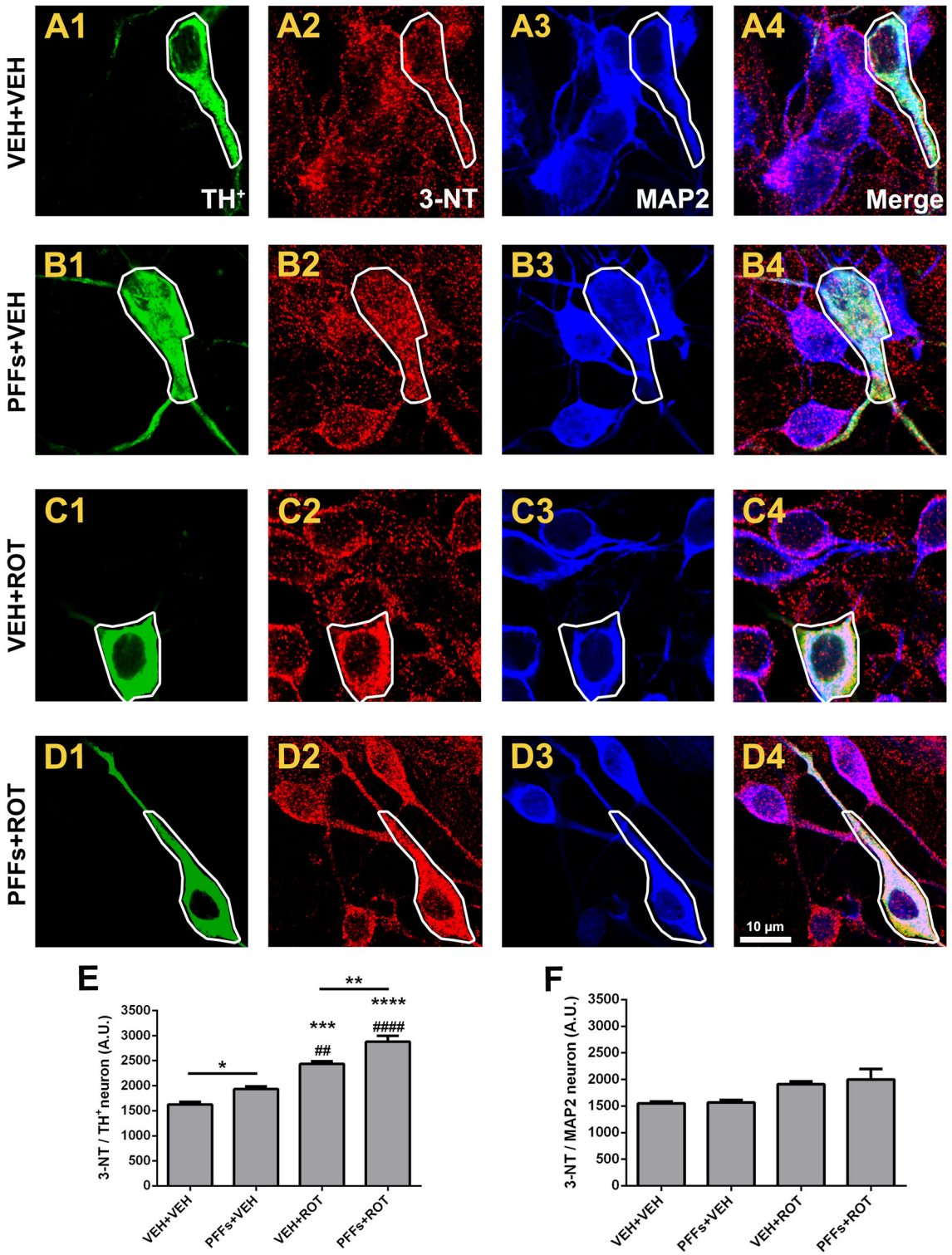

Fig. 8 Selective protein nitration in dopamine-positive neurons. **a–d** High-resolution confocal images acquired with a 100× objective and zoomed in three times revealed that PFFs enhanced 3-NT immunoreactivity in DA neurons either alone (**b2**) or after rotenone exposure (**d2**), whereas no meaningful fluorescence changes were noticed in non-DA neurons. **e** Quantitative analysis showing an increase of 3-NT fluorescence intensity after PFFs, rotenone, and PFFs + ROT administration in DA neurons. **f** Histogram depicting 3-NT protein levels in non-DA neurons. Data are presented as mean ± SEM carried out in triplicate in three separate wells per condition. A total of ~25–30 TH^+ and 500–600 MAP2 neurons per group were analyzed. $^{****}p < 0.0001$, $^{***}p < 0.001$, $^{*}p < 0.05$ compared to VEH + VEH. $^{\#\#\#\#}p < 0.0001$ and $^{\#\#}p < 0.01$ relative to PFFs + VEH. $^{**}p < 0.01$ and $^{**}p < 0.05$ vs. VEH + ROT (one-way ANOVA followed by Newman–Keuls multiple comparisons test). *Scale bar* 10 µm

generation in SH-SY5Y cells [44]. Our data revealed an important upregulation of mitochondrial ROS and deficits in mitochondrial respiration function.

Cumulative evidence has shown that α-syn plays a central role in regulating mitochondrial dynamics and function. Overexpression of human wild-type α-syn produced mitochondrial fragmentation and excessive mitophagy in SH-SY5Y cells [28]. Upregulated expression of human wild-type α-syn may promote fission by both Drp1-dependent or -independent pathways and subsequent changes in mitochondrial morphology [29]. Our findings here show that PFFs downregulated Opa1 levels, which may result in reduced fusion and culminate in perturbed mitochondrial fission–fusion cycle. Nitration may also represent a mechanism whereby α-syn polymerizes into filamentous aggregates. Inclusions assembled in nitrated HEK293 cells overexpressing α-syn stained positive against 3-NT epitope [45]. Antibodies directed against specific nitrated tyrosine residues revealed an extensive nitration of α-syn in patients with underlying LB pathology [3, 46]. It has been suggested that α-syn may mediate neurotoxicity downstream of mitochondrial complex I inhibition by stimulating the synthesis of mitochondrial $NO^{\cdot}$ and 3-NT [11]. In this work, we show that PFFs triggered selective enhancement of 3-NT levels in DA neurons.

Early microglial activation can be mediated by α-syn and this interaction results in a proliferation of a subset of proinflammatory markers. TNF-α release and NF-κB p65 nuclear translocation were observed in BV2 cells after α-syn incubation [47]. In the same study, microinjection of α-syn followed by systemic LPS administration into mice SN provoked microglial activation and upregulation in the mRNA levels of several proinflammatory cytokines and inflammatory markers. AAV2-mediated overexpression of human α-syn into mouse SN induced microglial activation, resulting in augmented $CD68^{+}$ cell immunoreactivity, lymphocyte number, and the expression of some proinflammatory cytokines [48]. Elevated expression of TNF-α and microglial activation were noticed in both the striatum and SN of young Thy1-αSyn mice [49]. Induced expression of double-mutant α-syn caused early activation of microglia in primary microglia-enriched cell cultures and SN DA neurons of transgenic mice [50]. We identified that PFFs induced an inflammatory response although microglial cells continued inactivated.

Specific derangements in complex I are responsible for increased α-syn fibrillation and might directly contribute to DA degeneration. Thus, accumulated α-syn in striatal and SN mitochondria of postmortem late-onset PD brains exhibited a threefold decrement in complex I activity [8]. The pesticide rotenone was able to accelerate the kinetics of α-syn fibrillation in a concentration-sensitive fashion [51]. Despite uniform systemic inhibition of mitochondrial complex I, rotenone upregulates endogenous expression of α-syn, produces cytoplasmic inclusions, and exacerbates ROS production, leading to selective DA neuronal demise [17–19, 52]. As evidence for rotenone-induced oxidative stress, protein thiol oxidation and increased mitochondrial superoxide anion were observed in DA neurons of several biological systems [53]. Chronic administration of rotenone to transgenic rats expressing E46 K human α-syn or G2019S leucine-rich repeated kinase 2 exhibited significantly higher oxidative and nitrosative damage relative to their respective wild-type littermates [54, 55].

To the best of our knowledge, there is only one report testing the influence of rotenone on SNARE proteins in which SNAP-25 and syntaxin levels were declined in PC12 cells [56]. In addition, dampened axonal and dendritic mitochondrial trafficking were observed in cortical neuron cultures following rotenone exposure [57]. Considerable evidence substantiates the involvement of DNA damage in rotenone toxicity [18]. Prolonged rotenone exposure altered mitochondrial dynamics, leading to an early activation of fusion events and an augmented fission processes in later stages [57]. It has been established that microglia is directly implicated in rotenone DA neuronal loss in vitro and in vivo [19, 58]. Mild increase in astrocyte population might also be linked to rotenone-induced DA neuronal loss [20, 21]. In this work, rotenone caused a marked reduction in the expression of synaptic- and axonal transport-related proteins, increase in DNA DBS and oxidative stress, impaired mitochondrial function, inflammatory response, and DA cell loss.

Our study also provides insight into the molecular mechanisms that underlie PFFs-mediated selective DA neuronal loss, which seem to be independent of the complex I inhibition and concomitant oxidative stress caused by rotenone. Our demonstration that 3-NT expression was selectively enhanced in DA cells upon fibrils administration is suggestive of $NO^{\cdot}$ involvement in the PFFs toxic process. Basal levels of nNOS mRNA, protein expression, and enzyme activity are markedly low in ventral midbrain DA neurons—it is practically restricted to a subpopulation of GABA-synthesizing neurons in the SN pars reticulata [59, 60]. In a healthy brain, iNOS is undetectable but under pathological conditions is transcriptionally upregulated by inflammatory stimuli in neuronal and glial cells, thereby producing sustained large amounts of $NO^{\cdot}$. Experimental and clinical evidence have shown that iNOS is highly expressed in SN DA neurons compared to control group; genetic ablation and pharmacological inhibition of iNOS significantly attenuated DA toxicity in a MPTP mouse model of PD, suggesting that iNOS plays a key role in the degeneration of the nigrostriatal DA system [30, 61]. Our study provided clear evidence that iNOS-derived $NO^{\cdot}$ is

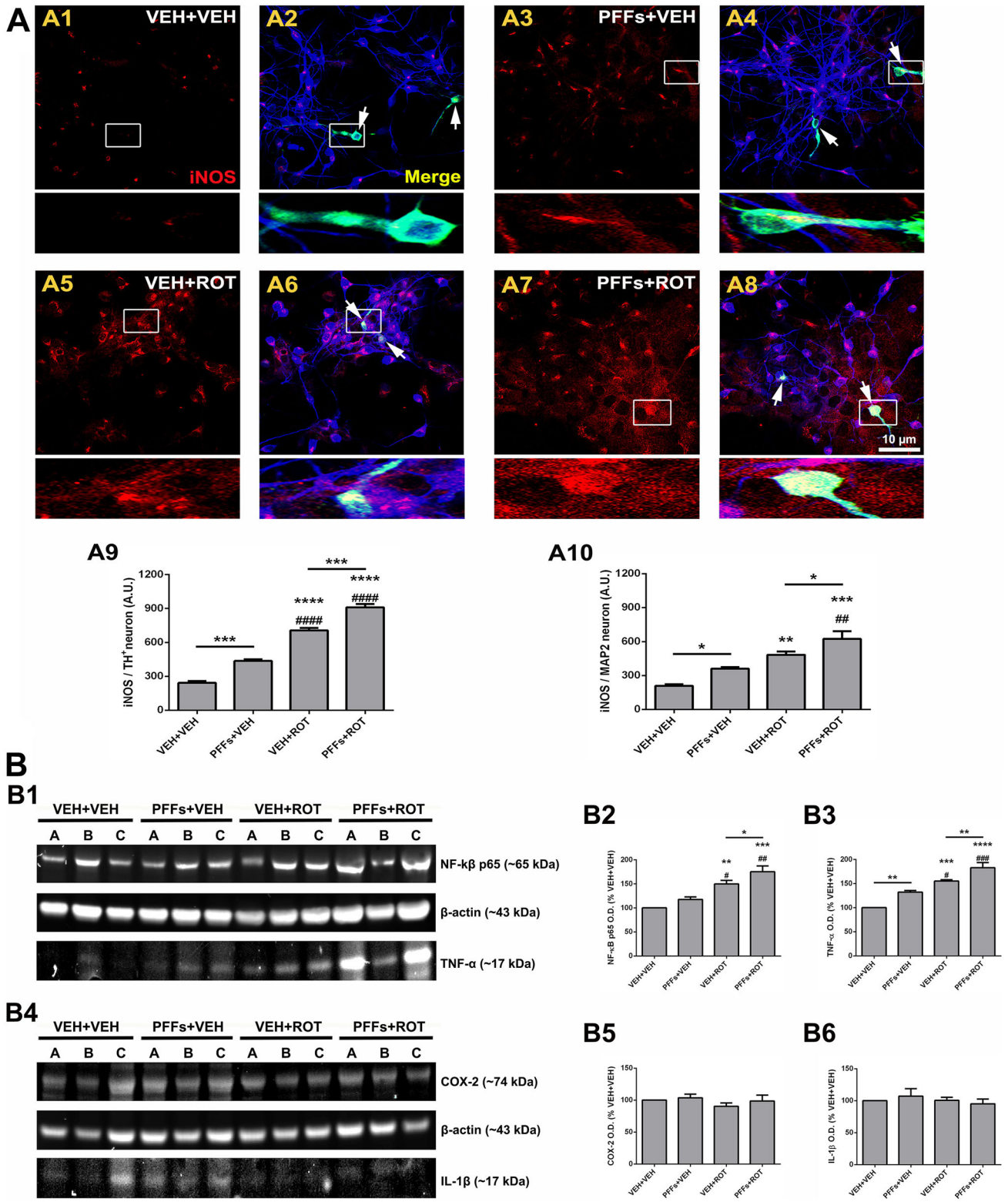
A
A1
VEH+VEH
iNOS
A2
Merge
A3
PFFs+VEH
A4
A5
VEH+ROT
A6
A7
PFFs+ROT
A8
10 µm
A9
iNOS / TH+ neuron (A.U.)
A10
iNOS / MAP2 neuron (A.U.)
VEH+VEH
PFFs+VEH
VEH+ROT
PFFs+ROT
B
B1
A B C A B C A B C A B C
NF-kβ p65 (~65 kDa)
β-actin (~43 kDa)
TNF-α (~17 kDa)
B2
NF-κB p65 O.D. (% VEH+VEH)
B3
TNF-α O.D. (% VEH+VEH)
B4
COX-2 (~74 kDa)
β-actin (~43 kDa)
IL-1β (~17 kDa)
B5
COX-2 O.D. (% VEH+VEH)
B6
IL-1β O.D. (% VEH+VEH)

◀**Fig. 9** Inflammatory response. **a** Confocal microscopy micrographs acquired with the 60× lens from cells stained with primary antibodies against iNOS (*red*), TH^+ (*green*), and MAP2 (*blue*). Faint iNOS immunoreactivity was detected in the vehicle group (**a1**, **a2**); however, PFFs caused an enhancement of iNOS levels in the neuropil and neurons (**a3**, **a4**). iNOS expression was substantially raised after neuronal exposure to rotenone (**a5**, **a6**). This effect was even more prominent in the PFFs plus rotenone group (**a7**, **a8**). Graphical representation of iNOS expression levels in DA (**a9**) and non-DA (**a10**) neurons. Data are averages of the mean fluorescence intensity of triplicate samples ± SEM ($n = 3$). An average of ~25–30 TH^+ and 250–450 MAP2 neurons per group were analyzed. $^{****}p < 0.0001$, $^{***}p < 0.001$, $^{**}p < 0.01$, and $^{*}p < 0.05$ vs. VEH + VEH. $^{\#\#\#\#}p < 0.0001$ and $^{\#\#}p < 0.01$ compared to PFFs + VEH. $^{***}p < 0.001$ and $^{*}p < 0.05$ relative to VEH + ROT (one-way ANOVA followed by Newman–Keuls multiple comparisons test). *Scale bar* 10 μm. **b** Representative immunoblots depicting expression of TNF-α and NF-κB subunit p65 (**b1**) and COX-2 and IL-1β (**b4**). Densitometric analysis revealed that PFFs administration resulted in an upregulation of p65 catalytic subunit of the transcription factor NF-κB (**b2**) and the cytokine TNF-α (**b3**). Contrarily, optical density values of COX-2 (**b5**) and IL-1β (**b6**) remained unaffected. Values are presented as from three independent cultures in triplicate and are expressed as mean optical densitometry ± SEM. *Bars* represent proinflammatory marker levels calculated as percentage of their respective controls (i.e., VEH + VEH group). $^{****}p < 0.0001$, $^{***}p < 0.001$, and $^{**}p < 0.01$ compared to VEH + VEH. $^{\#\#\#}p < 0.001$, $^{\#\#}p < 0.01$, and $^{\#}p < 0.05$ vs. PFFs + VEH. $^{**}p < 0.01$ and $^{*}p < 0.05$ relative to VEH + ROT (one-way ANOVA followed by Newman–Keuls multiple comparisons test)

directly implicated in PFFs pathogenicity and abrogated inflammation via downregulation of iNOS expression and concomitant oxidative stress preserves DA neurons against PFFs-induced toxicity. These findings are in agreement with a previous report where α-syn (but not tau) PFFs provoked lysosomal NADPH oxidase activity, resulting in enhanced ROS production in the cytosol and subsequent increase in mitochondrial matrix oxidative stress, which was significantly reduced in neurons incubated with L-NAME, a non-isoform-specific inhibitor that binds to NOS irreversibly [62].

In summary, we have developed, validated, and characterized a novel and reliable in vitro experimental model to study DA-related neurodegeneration, in which several pathological key features of the disease were successfully recapitulated. Further investigation is necessary to determine whether these findings have significant implications in vivo.

Materials and methods

Preparation and transduction of recombinant α-synuclein fibrils

Recombinant full length human α-syn was expressed in BL21 cells and purified as previously described [63]. Briefly, PFFs were assembled by incubating α-syn at 37 °C for 7 days [6]. Constant agitation at 1000 rpm was maintained using a thermomixer. Completed reactions were aliquoted and stored at −80 °C.

Primary dopamine neuron cultures

Neuron cultures were prepared from embryonic day 17 Sprague-Dawley rats (Charles River, Wilmington, MA, USA). Embryos were obtained from 2–3 pregnant dams. Pooled ventral midbrain tissue was dissociated with enzymatic digestion using trypsin followed by mechanical trituration. Cells were seeded at 5×10^5/well density in a 24-well plate. The cultures were maintained at 37 °C in a humidified atmosphere of 5% CO_2 and 95% air in MEM with 2% FBS, 2% HS, 1 g/L glucose, 2 mM GlutaMax, 100 μM non-essential amino acids, 1 mM sodium pyruvate, 50 U/mL penicillin, and 50 μg/mL streptomycin. After 48 h, the culture medium was replaced with serum-free Neurobasal medium containing 0.5 mg/mL AlbuMAX I, 2 mM GlutaMAX I, 2% B27 supplement, 50 U/mL penicillin, and 50 μg/mL streptomycin. 50 ng/mL GDNF (#512-GF-050; R&D Systems. Minneapolis, MN, USA) was also added. Five days after seeding, the media was removed and replenished with neurobasal medium, GDNF, PFFs, and rotenone (≥95%, Sigma-Aldrich. St. Louis, MO, USA). At 9 DIV, fresh neurobasal medium was added over old medium in combination with GDNF. At 13 DIV, 70% of old medium was replaced. All procedures were performed with the approval of the University of Pittsburgh Animal Care and Use Committee.

Experimental design

Single-dose administration of PFFs, rotenone, or vehicle was used to treat neuronal cultures at 5 DIV. PFFs stock solutions (5 mg/mL; concentration of monomer equivalent) were thawed to room temperature (RT), prepared in sterile 1× PBS (0.1 mg/mL), and diluted in neuronal media at the final desired concentration. To improve seeding activity and normalize fibril size/length, PFFs were fragmented through sonication (65 pulses over 40 s at power level 2). For a 24-well tray, 2 μg/mL of PFFs were added to each well, whereas 5 μg/mL of α-syn PFFs per well were added to the Seahorse 96-well microplates. Rotenone was freshly prepared in DMSO and diluted to appropriate final concentration (50 nM) in fresh Neurobasal medium. Nineteen days after seeding—14 days of PFFs treatment—the cultures were fixed and processed for subsequent analysis (unless otherwise noted).

Immunocytochemistry

At the end of the culture period, cells were fixed in 4% PFA, 0.02% Triton, and 1 mM $MgCl_2$ in PBS for 30 min.

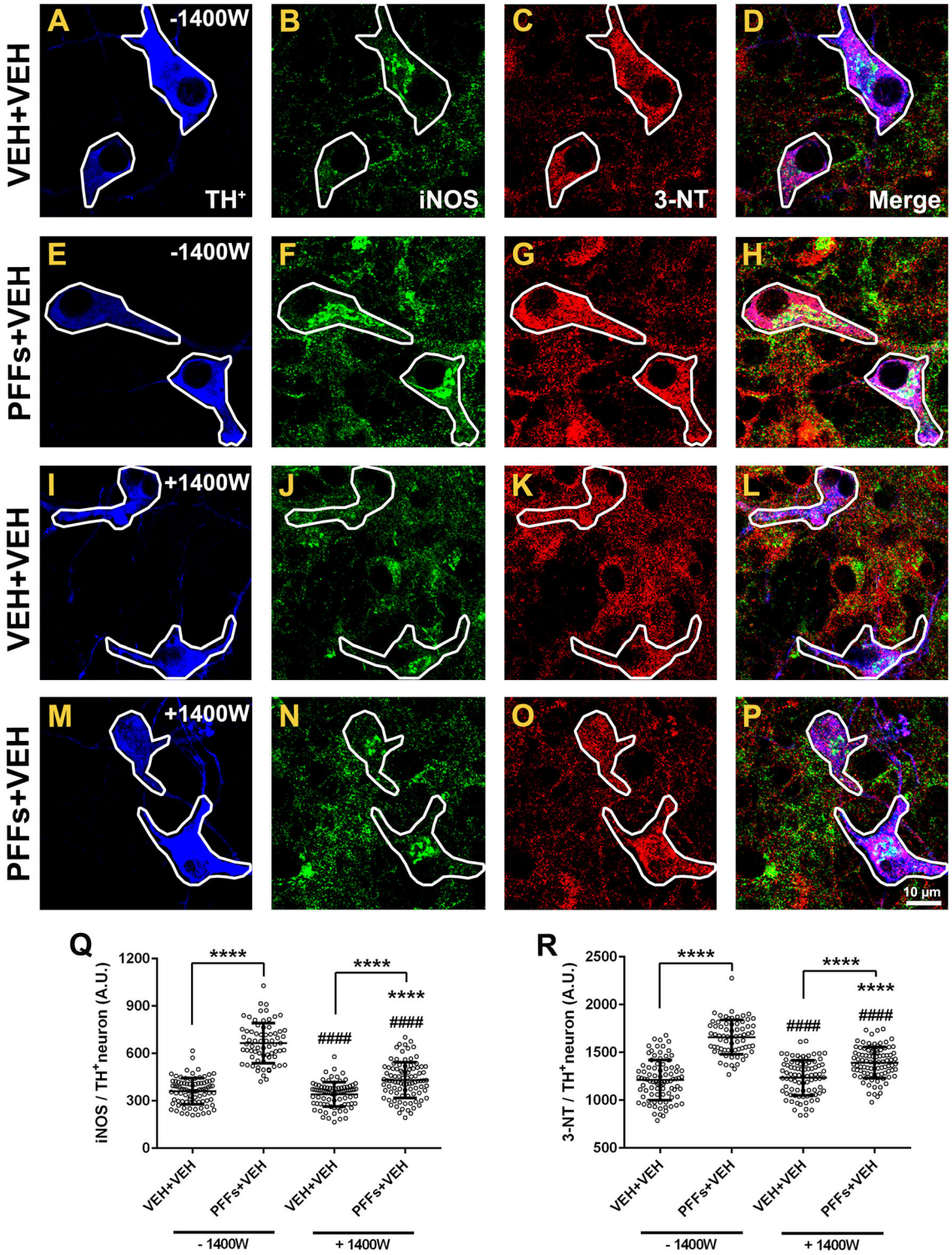

Fig. 10 1400 W downregulates iNOS expression and attenuates protein tyrosine nitration. **a** High-resolution confocal images displaying a substantial enhancement of iNOS (*green*) and 3-NT (*red*) fluorescence intensity following PFFs exposure (**b** vs. **f** and **c** vs. **g**, respectively). These effects were abolished in neurons exposed to 1400 W plus PFFs (**j** vs. **n** and **k** vs. **o**, respectively). Scatter plots illustrating average individual values per group of iNOS (**q**) and 3-NT (**r**) protein levels. Data values are shown as mean ± SEM. The experiment was done triplicate from two independent datasets. An average of ~40–60 TH^+ neurons were tested. *Scale bar* 10 µm. $^{****}p < 0.0001$ vs. VEH + VEH (−1400 W). $^{\#\#\#\#}p < 0.0001$ vs. PFFs + VEH (−1400 W). $^{****}p < 0.0001$ vs. VEH + VEH (+1400 W) (one-way ANOVA followed by Newman–Keuls multiple comparisons test)

First, neurons were washed trice in PBS for 10 min each. Unless otherwise stated, all incubations were carried out at RT. After blocking with a solution consisting in 10% normal donkey serum in PBS for 1 h, the cultures were incubated in primary antibodies (Table S1) in PBS with 1% normal donkey serum overnight at 4 °C. Next, neuronal cultures were rinsed 3 times in PBS for 10 min each and subsequently incubated with conjugated secondary antibodies (Table S2) in PBS with 1% normal donkey serum for 2 h. Neurons were washed once in PBS followed by H 33342 (1:3000) counterstaining for 5 min. Lastly, after three rinses in PBS for 10 min, the samples were mounted directly onto plus-coated slides and coverslipped using gelvatol mounting media.

Sequential extraction and western blotting

Neurons were washed twice in sterile 1× PBS and scraped from the dish into ice-cold 1× sample buffer plus the halt protease and phosphatase inhibitor cocktail containing 0.5 M EDTA. Harvested cells were sonicated, and protein concentrations were determined. Lysates were either used immediately or stored at −80 °C until experiment. Neuronal lysates were incubated with precipitant solution and cleared by centrifugation at 13,200 rpm for 10 min at 4 °C. The pellets were resolved in 4× reducing loading buffer and sample reducing agent and boiled for 3 min at 95–100 °C. Equivalent amounts of total protein from each lysate were loaded and separated on a 4–12% SDS-PAGE gradient gel. After electrophoresis, proteins were transferred onto a nitrocellulose membrane in transfer buffer and then, immunoblotted with primary antibodies (Table S1) diluted in blocking buffer solution (#927-40000, LI-COR Biosciences, Lincoln, Nebraska, USA) overnight at 4 °C. Washed membranes (3 times in PBS for 10 min) were incubated with the corresponding infrared dye-conjugated secondary antibodies (Table S2) for 1 h and rinsed four times with PBS. The respective proteins were detected using the LI-COR Odyssey CLx infrared imaging system, and the optical band densities were quantified and normalized to β-actin levels (used as internal control).

Mitochondrial respiration

Cellular oxygen consumption rate (OCR) was measured using an extracellular flux analyzer (Seahorse Bioscience. North Billerica, MA, USA) as described previously with the following modifications [64]. Intact primary ventral midbrain neurons were grown in XF96 plates seeded at 80,000 cells/well for one week in growth medium. Neuronal cultures were then treated with either vehicle (PBS) or PFFs (5 μg/mL) for 72 h. Next, plates were incubated in the same growth medium but the Neurobasal medium was replaced to DMEM with high glucose for 1 h at 37 °C. Media containing final concentrations of 10 μM oligomycin, 300 nM FCCP, 1 μM rotenone, and 1 μM antimycin-A were pre-loaded into the drug delivery system. Once the basal OCR was measured, the compounds were added sequentially and the effects on OCR measured every 8 min. All experiments were carried out a minimum of three to five times.

High-resolution confocal laser scanning microscopy analysis

Fluorescent images were acquired under constant power and pinhole aperture on an Olympus BX61 confocal microscope and evaluated using the Fluoview Viewer Olympus software package (v. 2.1c). Quantitative analysis of mitochondrial dynamic-associated protein fluorescence intensity, 3-NT levels, iNOS expression, and Pearson's correlation was performed with an UPlanSApo 60× (N.A. 1.35) oil-immersion objective lens. Synuclein recruitment, time-dependent aggregation study, LB localization, synaptic protein immunoreactivity, axonal transport motor protein expression, DNA damage, and mitochondrial mass fluorescence intensity were examined using the UPlanSApo 100× (N.A. 1.4) oil-immersion objective. Regions of interest (ROI) were drawn around the somata of DA (TH^+, tyrosine hydroxylase) and non-DA neurons (MAP2, microtubule-associated protein 2). For the assessment of axonal transport- and mitochondrial dynamic-related protein expression levels, ROI were outlined including both perikaryon and axons. Imaging was carried out under identical and specific acquisition settings for the individual fluorophores. The mean intensity value was calculated for each ROI. At least, three independent experiments were examined for each condition.

Mitochondrial ROS measurement in living neurons

The mitochondria-specific ROS fluorogenic indicator, MitoSOX Red (#M36008, Life Technologies. Carlsbad, CA, USA), was employed to label and measure $O_2^{\cdot-}$ production by live-cell imaging. For the analysis, Neurobasal medium was replaced with buffer solution containing 1× HBSS, 1× $CaCl_2$, 1× $MgSO_4$, glucose, and $NaHCO_3$ at 37 °C. MitoSOX was used at a final concentration of 0.5 μM. Rotenone was added at a final concentration of 10 or 100 nM. MitoSOX fluorescence was recorded using an excitation filter of 510 nm and an emission filter of 580 nm in a Leica microscope using an epifluorescence Plan Apo 40× (N.A. 1.25) oil-immersion objective. Images were collected with an ORCA-ER CCD camera and assessed using the Hamamatsu Simple PCI software package (v. 6.6). The signal was normalized with baseline fluorescence

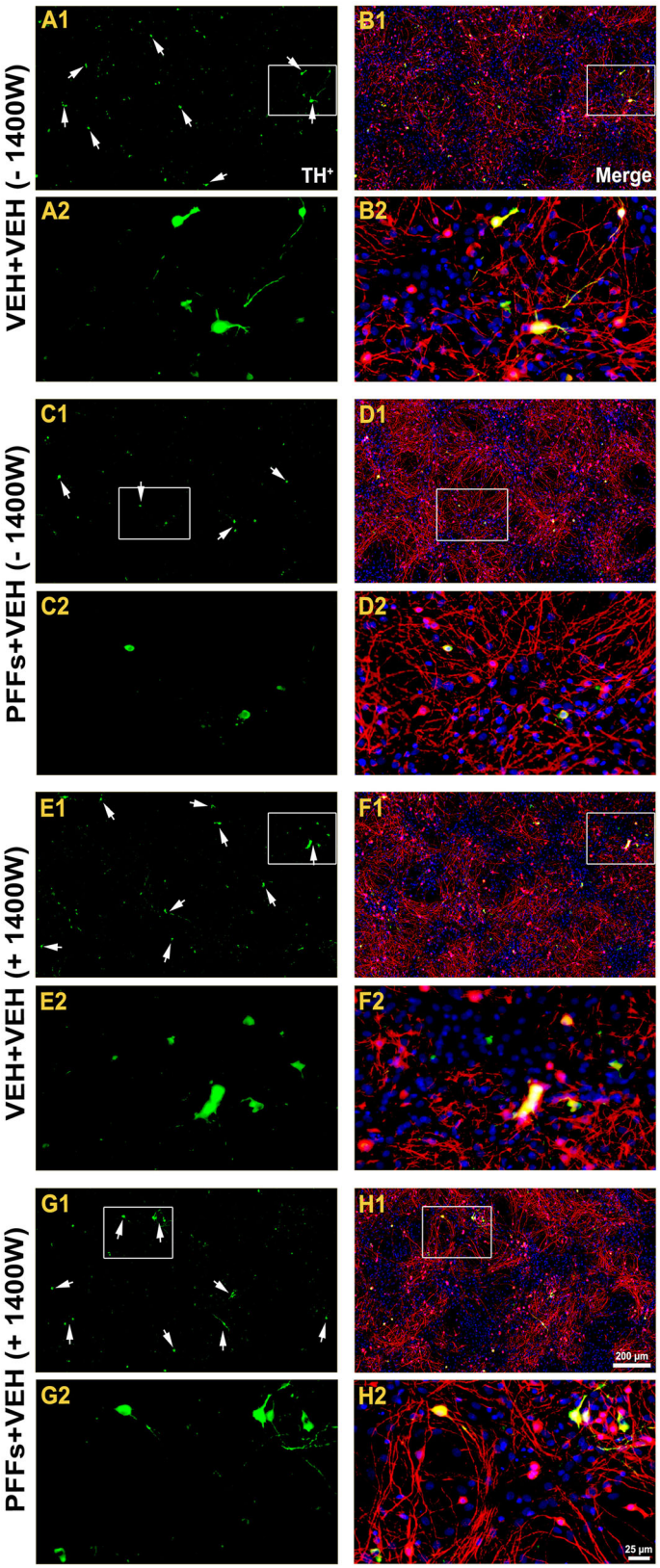
VEH+VEH (- 1400W)
PFFs+VEH (- 1400W)
VEH+VEH (+ 1400W)
PFFs+VEH (+ 1400W)
A1
B1
TH+
Merge
A2
B2
C1
D1
C2
D2
E1
F1
E2
F2
G1
H1
G2
H2
200 µm
25 µm

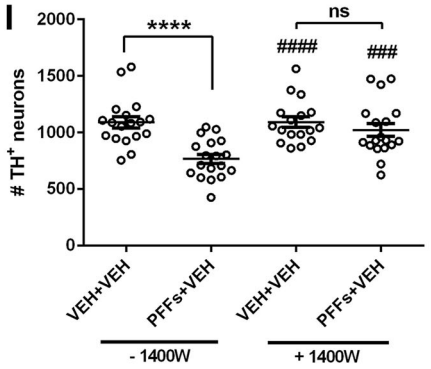
I
TH+ neurons
2000
1500
1000
500
0
****
ns
####
###
VEH+VEH
PFFs+VEH
VEH+VEH
PFFs+VEH
- 1400W
+ 1400W

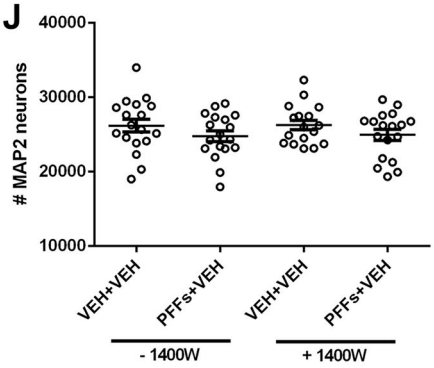
J
MAP2 neurons
40000
30000
20000
10000
VEH+VEH
PFFs+VEH
VEH+VEH
PFFs+VEH
- 1400W
+ 1400W

◀**Fig. 11** 1400 W protects against PFFs-induced dopamine neuron loss. Neuron cultures were stained with antibodies against TH^+ (*green*) and MAP2 (*red*) and nuclear counterstain with H 33342 (*blue*). Qualitative assessment indicated a decrease in TH^+ neuronal population in cells treated with PFFs compared to control group (**a**, **b** vs. **c**, **d**). Pretreatment with 1400 W followed by PFFs significantly preserved the number of TH^+ neurons (**e**, **f** vs. **g**, **h**). Unbiased neuronal counting revealed that, in the absence of 1400 W, there was a significant decline in TH^+ population (~30%) following PFFs treatment (**i**), whereas no changes were noticed in the number of MAP2 neurons (**j**). Contrarily, cultures incubated in the presence of 1400 W displayed an important degree of neuroprotection against PFFs-induced overt DA neuron demise. Data from four independent cultures in triplicate were combined to determine mean ± SEM. *Scale bar* 200 μm; *insets* 25 μm. $^{****}p < 0.0001$ vs. VEH + VEH (−1400 W). $^{\#\#\#\#}p < 0.0001$ and $^{\#\#\#}p < 0.001$ vs. PFFs + VEH (−1400 W) (one-way ANOVA followed by Newman–Keuls multiple comparisons test)

detected before PFFs or rotenone application. Values were pooled from three independent datasets performed in triplicate.

Unbiased neuronal cell counts

For neuron quantification, we used our recently reported automated imaging system [20, 21]. The motorized stage approach allows the acquisition of multiple channels (blue, green, red, far red, and near IR) over several stage positions, creating large-field-of-view datasets that are automatically stitched together to generate extremely high-resolution montages. Fluorescent images stained with anti-TH^+ and -MAP2 antibodies and counterstained with Hoechst 33342 were collected on a Nikon 90i upright fluorescence microscope equipped with a linear encoded motorized stage using the 20× (N.A. 0.75) objective lens. Data analysis of the central region of the coverslip (to disregard cell aggregation and fluorescence saturation located in the edges) was performed using the Nikon NIS-Elements software package (v. 4.30). All slides were scanned under the same conditions for magnification, camera gain, lamp intensity, and exposure time. Image acquisition and data analysis were carried out by a single trained investigator. All experiments were repeated four times with each sample prepared in triplicate.

Microglial analysis

Immunofluorescent images from DA neuron cultures were assembled on an automated Nikon 90i wide-field microscope at 20×. Then, digital pictures were exported and analyzed with ImageJ software (v. 1.48) where RGB color images were converted into 8-bit grayscale files with pixel values ranging from 0 to 255. After creating ROIs, background was subtracted and the average pixel intensity was calculated. Values for microglial morphology, number of microglial-positive cells, and the area occupied by microglia over the total area were generated. Data from three independent cultures in triplicate were combined.

Data analysis and statistics

Statistical analyses were performed with GraphPad Prism 6.0 software. Unless otherwise stated, all data were expressed as mean values ± SEM. Parametric ANOVA with the Newman–Keuls post hoc correction was undertaken to determine pairwise comparisons among multiple datasets. Mitochondrial respiration was analyzed using unpaired Student *t* test after testing for Gaussian distribution. For all tests, $p < 0.05$ was deemed significant.

Acknowledgements This work was supported by the DSF Charitable Foundation, the Consolidated Anti-Aging Foundation, the National Institutes of Health (NS059806, NS095387, ES020718, ES020327), the Blechman Foundation, and the American Parkinson Disease Association. The authors would like to thank Dr. Simon Watkins (Center for Biologic Imaging, University of Pittsburgh, PA, USA) for the use of the motorized stage system and Evan Howlett for technical assistance.

Author contributions VT contributed to the design and conceptualization of the study and complete data collection, analysis and interpretation of data, drafting and revision of the manuscript. XH carried out the cell culture. KCL synthesized the PFFs and contributed to interpretation of the data and revision of the manuscript. LHS performed the mitochondrial respiration assays. VML assisted with manuscript revision. JTG participated in the design and conceptualization of the study, data interpretation, and revision of the manuscript.

Compliance with ethical standards

Conflict of interest The authors declare that there are no actual or potential conflicts of interest, including any financial, personal, or other relationships with people or organizations during the development of the work submitted.

References

1. Anderson JP, Walker DE, Goldstein JM, de Laat R, Banducci K, Caccavello RJ, Barbour R, Huang J, Kling K, Lee M, Diep L, Keim PS, Shen X, Chataway T, Schlossmacher MG, Seubert P, Schenk D, Sinha S, Gai WP, Chilcote TJ (2006) Phosphorylation of Ser-129 is the dominant pathological modification of alpha-synuclein in familial and sporadic Lewy body disease. J Biol Chem 281(40):29739–29752. doi:10.1074/jbc.M600933200
2. Fujiwara H, Hasegawa M, Dohmae N, Kawashima A, Masliah E, Goldberg MS, Shen J, Takio K, Iwatsubo T (2002) alpha-Synuclein is phosphorylated in synucleinopathy lesions. Nat Cell Biol 4(2):160–164. doi:10.1038/ncb748
3. Giasson BI, Duda JE, Murray IV, Chen Q, Souza JM, Hurtig HI, Ischiropoulos H, Trojanowski JQ, Lee VM (2000) Oxidative damage linked to neurodegeneration by selective alpha-synuclein nitration in synucleinopathy lesions. Science 290(5493):985–989
4. Hamza TH, Zabetian CP, Tenesa A, Laederach A, Montimurro J, Yearout D, Kay DM, Doheny KF, Paschall J, Pugh E, Kusel VI,

Collura R, Roberts J, Griffith A, Samii A, Scott WK, Nutt J, Factor SA, Payami H (2010) Common genetic variation in the HLA region is associated with late-onset sporadic Parkinson's disease. Nat Genet 42(9):781–785. doi:10.1038/ng.642

5. Simon-Sanchez J, Schulte C, Bras JM, Sharma M, Gibbs JR, Berg D, Paisan-Ruiz C, Lichtner P, Scholz SW, Hernandez DG, Kruger R, Federoff M, Klein C, Goate A, Perlmutter J, Bonin M, Nalls MA, Illig T, Gieger C, Houlden H, Steffens M, Okun MS, Racette BA, Cookson MR, Foote KD, Fernandez HH, Traynor BJ, Schreiber S, Arepalli S, Zonozi R, Gwinn K, van der Brug M, Lopez G, Chanock SJ, Schatzkin A, Park Y, Hollenbeck A, Gao J, Huang X, Wood NW, Lorenz D, Deuschl G, Chen H, Riess O, Hardy JA, Singleton AB, Gasser T (2009) Genome-wide association study reveals genetic risk underlying Parkinson's disease. Nat Genet 41(12):1308–1312. doi:10.1038/ng.487
6. Luk KC, Song C, O'Brien P, Stieber A, Branch JR, Brunden KR, Trojanowski JQ, Lee VM (2009) Exogenous alpha-synuclein fibrils seed the formation of Lewy body-like intracellular inclusions in cultured cells. Proc Natl Acad Sci USA 106(47):20051–20056. doi:10.1073/pnas.0908005106
7. Volpicelli-Daley LA, Luk KC, Patel TP, Tanik SA, Riddle DM, Stieber A, Meaney DF, Trojanowski JQ, Lee VM (2011) Exogenous alpha-synuclein fibrils induce Lewy body pathology leading to synaptic dysfunction and neuron death. Neuron 72(1):57–71. doi:10.1016/j.neuron.2011.08.033
8. Devi L, Raghavendran V, Prabhu BM, Avadhani NG, Anandatheerthavarada HK (2008) Mitochondrial import and accumulation of alpha-synuclein impair complex I in human dopaminergic neuronal cultures and Parkinson disease brain. J Biol Chem 283(14):9089–9100. doi:10.1074/jbc.M710012200
9. Perez RG, Waymire JC, Lin E, Liu JJ, Guo F, Zigmond MJ (2002) A role for alpha-synuclein in the regulation of dopamine biosynthesis. J Neurosci 22(8):3090–3099
10. Hsu LJ, Sagara Y, Arroyo A, Rockenstein E, Sisk A, Mallory M, Wong J, Takenouchi T, Hashimoto M, Masliah E (2000) Alpha-synuclein promotes mitochondrial deficit and oxidative stress. Am J Pathol 157(2):401–410
11. Parihar MS, Parihar A, Fujita M, Hashimoto M, Ghafourifar P (2008) Mitochondrial association of alpha-synuclein causes oxidative stress. Cell Mol Life Sci 65(7–8):1272–1284. doi:10.1007/s00018-008-7589-1
12. Venda LL, Cragg SJ, Buchman VL, Wade-Martins R (2010) Alpha-synuclein and dopamine at the crossroads of Parkinson's disease. Trends Neurosci 33(12):559–568. doi:10.1016/j.tins.2010.09.004
13. Kim C, Ho DH, Suk JE, You S, Michael S, Kang J, Joong Lee S, Masliah E, Hwang D, Lee HJ, Lee SJ (2013) Neuron-released oligomeric alpha-synuclein is an endogenous agonist of TLR2 for paracrine activation of microglia. Nat Commun 4:1562. doi:10.1038/ncomms2534
14. Lee HJ, Suk JE, Patrick C, Bae EJ, Cho JH, Rho S, Hwang D, Masliah E, Lee SJ (2010) Direct transfer of alpha-synuclein from neuron to astroglia causes inflammatory responses in synucleinopathies. J Biol Chem 285(12):9262–9272. doi:10.1074/jbc.M109.081125
15. Zhang W, Wang T, Pei Z, Miller DS, Wu X, Block ML, Wilson B, Zhang W, Zhou Y, Hong JS, Zhang J (2005) Aggregated alpha-synuclein activates microglia: a process leading to disease progression in Parkinson's disease. FASEB J 19(6):533–542. doi:10.1096/fj.04-2751com
16. Betarbet R, Canet-Aviles RM, Sherer TB, Mastroberardino PG, McLendon C, Kim JH, Lund S, Na HM, Taylor G, Bence NF, Kopito R, Seo BB, Yagi T, Yagi A, Klinefelter G, Cookson MR, Greenamyre JT (2006) Intersecting pathways to neurodegeneration in Parkinson's disease: effects of the pesticide rotenone on DJ-1, alpha-synuclein, and the ubiquitin-proteasome system. Neurobiol Dis 22(2):404–420. doi:10.1016/j.nbd.2005.12.003
17. Cannon JR, Tapias V, Na HM, Honick AS, Drolet RE, Greenamyre JT (2009) A highly reproducible rotenone model of Parkinson's disease. Neurobiol Dis 34(2):279–290
18. Sherer TB, Betarbet R, Stout AK, Lund S, Baptista M, Panov AV, Cookson MR, Greenamyre JT (2002) An in vitro model of Parkinson's disease: linking mitochondrial impairment to altered alpha-synuclein metabolism and oxidative damage. J Neurosci 22(16):7006–7015
19. Tapias V, Cannon JR, Greenamyre JT (2014) Pomegranate juice exacerbates oxidative stress and nigrostriatal degeneration in Parkinson's disease. Neurobiol Aging 35(5):1162–1176. doi:10.1016/j.neurobiolaging.2013.10.077
20. Tapias V, Greenamyre JT (2014) A rapid and sensitive automated image-based approach for in vitro and in vivo characterization of cell morphology and quantification of cell number and neurite architecture. Curr Protoc Cytom 68:12 33 11–12 33 22. doi:10.1002/0471142956.cy1233s68
21. Tapias V, Greenamyre JT, Watkins SC (2013) Automated imaging system for fast quantitation of neurons, cell morphology and neurite morphometry in vivo and in vitro. Neurobiol Dis 54:158–168. doi:10.1016/j.nbd.2012.11.018
22. Luk KC, Kehm V, Carroll J, Zhang B, O'Brien P, Trojanowski JQ, Lee VM (2012) Pathological alpha-synuclein transmission initiates Parkinson-like neurodegeneration in nontransgenic mice. Science 338(6109):949–953. doi:10.1126/science.1227157
23. Luk KC, Kehm VM, Zhang B, O'Brien P, Trojanowski JQ, Lee VM (2012) Intracerebral inoculation of pathological alpha-synuclein initiates a rapidly progressive neurodegenerative alpha-synucleinopathy in mice. J Exp Med 209(5):975–986. doi:10.1084/jem.20112457
24. Chu Y, Morfini GA, Langhamer LB, He Y, Brady ST, Kordower JH (2012) Alterations in axonal transport motor proteins in sporadic and experimental Parkinson's disease. Brain 135(Pt 7):2058–2073. doi:10.1093/brain/aws133
25. Schulz-Schaeffer WJ (2010) The synaptic pathology of alpha-synuclein aggregation in dementia with Lewy bodies, Parkinson's disease and Parkinson's disease dementia. Acta Neuropathol 120(2):131–143. doi:10.1007/s00401-010-0711-0
26. Baritaud M, Cabon L, Delavallee L, Galan-Malo P, Gilles ME, Brunelle-Navas MN, Susin SA (2012) AIF-mediated caspase-independent necroptosis requires ATM and DNA-PK-induced histone H2AX Ser139 phosphorylation. Cell Death Dis 3:e390. doi:10.1038/cddis.2012.120
27. Nakamura K (2013) alpha-Synuclein and mitochondria: partners in crime? Neurotherapeutics 10(3):391–399. doi:10.1007/s13311-013-0182-9
28. Kamp F, Exner N, Lutz AK, Wender N, Hegermann J, Brunner B, Nuscher B, Bartels T, Giese A, Beyer K, Eimer S, Winklhofer KF, Haass C (2010) Inhibition of mitochondrial fusion by alpha-synuclein is rescued by PINK1, Parkin and DJ-1. EMBO J 29(20):3571–3589. doi:10.1038/emboj.2010.223
29. Nakamura K, Nemani VM, Azarbal F, Skibinski G, Levy JM, Egami K, Munishkina L, Zhang J, Gardner B, Wakabayashi J, Sesaki H, Cheng Y, Finkbeiner S, Nussbaum RL, Masliah E, Edwards RH (2011) Direct membrane association drives mitochondrial fission by the Parkinson disease-associated protein alpha-synuclein. J Biol Chem 286(23):20710–20726. doi:10.1074/jbc.M110.213538
30. Tapias V, Escames G, Lopez LC, Lopez A, Camacho E, Carrion MD, Entrena A, Gallo MA, Espinosa A, Acuna-Castroviejo D (2009) Melatonin and its brain metabolite *N*(1)-acetyl-5-methoxykynuramine prevent mitochondrial nitric oxide synthase induction in parkinsonian mice. J Neurosci Res 87(13):3002–3010. doi:10.1002/jnr.22123

31. McCormack AL, Mak SK, Di Monte DA (2012) Increased alpha-synuclein phosphorylation and nitration in the aging primate substantia nigra. Cell Death Dis 3:e315. doi:10.1038/cddis.2012.50
32. Amschl D, Neddens J, Havas D, Flunkert S, Rabl R, Romer H, Rockenstein E, Masliah E, Windisch M, Hutter-Paier B (2013) Time course and progression of wild type alpha-synuclein accumulation in a transgenic mouse model. BMC Neurosci 14:6. doi:10.1186/1471-2202-14-6
33. Schell H, Hasegawa T, Neumann M, Kahle PJ (2009) Nuclear and neuritic distribution of serine-129 phosphorylated alpha-synuclein in transgenic mice. Neuroscience 160(4):796–804. doi:10.1016/j.neuroscience.2009.03.002
34. Burre J, Sharma M, Tsetsenis T, Buchman V, Etherton MR, Sudhof TC (2010) Alpha-synuclein promotes SNARE-complex assembly in vivo and in vitro. Science 329(5999):1663–1667. doi:10.1126/science.1195227
35. Chandra S, Gallardo G, Fernandez-Chacon R, Schluter OM, Sudhof TC (2005) Alpha-synuclein cooperates with CSPalpha in preventing neurodegeneration. Cell 123(3):383–396. doi:10.1016/j.cell.2005.09.028
36. Galvin JE, Uryu K, Lee VM, Trojanowski JQ (1999) Axon pathology in Parkinson's disease and Lewy body dementia hippocampus contains alpha-, beta-, and gamma-synuclein. Proc Natl Acad Sci USA 96(23):13450–13455
37. Chung CY, Koprich JB, Siddiqi H, Isacson O (2009) Dynamic changes in presynaptic and axonal transport proteins combined with striatal neuroinflammation precede dopaminergic neuronal loss in a rat model of AAV alpha-synucleinopathy. J Neurosci 29(11):3365–3373. doi:10.1523/JNEUROSCI.5427-08.2009
38. Muller SK, Bender A, Laub C, Hogen T, Schlaudraff F, Liss B, Klopstock T, Elstner M (2013) Lewy body pathology is associated with mitochondrial DNA damage in Parkinson's disease. Neurobiol Aging 34(9):2231–2233. doi:10.1016/j.neurobiolaging.2013.03.016
39. Martin LJ, Pan Y, Price AC, Sterling W, Copeland NG, Jenkins NA, Price DL, Lee MK (2006) Parkinson's disease alpha-synuclein transgenic mice develop neuronal mitochondrial degeneration and cell death. J Neurosci 26(1):41–50. doi:10.1523/JNEUROSCI.4308-05.2006
40. Decressac M, Mattsson B, Lundblad M, Weikop P, Bjorklund A (2012) Progressive neurodegenerative and behavioural changes induced by AAV-mediated overexpression of alpha-synuclein in midbrain dopamine neurons. Neurobiol Dis 45(3):939–953. doi:10.1016/j.nbd.2011.12.013
41. Baptista MJ, O'Farrell C, Daya S, Ahmad R, Miller DW, Hardy J, Farrer MJ, Cookson MR (2003) Co-ordinate transcriptional regulation of dopamine synthesis genes by alpha-synuclein in human neuroblastoma cell lines. J Neurochem 85(4):957–968
42. Kirik D, Rosenblad C, Burger C, Lundberg C, Johansen TE, Muzyczka N, Mandel RJ, Bjorklund A (2002) Parkinson-like neurodegeneration induced by targeted overexpression of alpha-synuclein in the nigrostriatal system. J Neurosci 22(7):2780–2791
43. Tanaka S, Takehashi M, Matoh N, Iida S, Suzuki T, Futaki S, Hamada H, Masliah E, Sugiura Y, Ueda K (2002) Generation of reactive oxygen species and activation of NF-kappaB by non-Abeta component of Alzheimer's disease amyloid. J Neurochem 82(2):305–315
44. Parihar MS, Parihar A, Fujita M, Hashimoto M, Ghafourifar P (2009) Alpha-synuclein overexpression and aggregation exacerbates impairment of mitochondrial functions by augmenting oxidative stress in human neuroblastoma cells. Int J Biochem Cell Biol 41(10):2015–2024. doi:10.1016/j.biocel.2009.05.008
45. Paxinou E, Chen Q, Weisse M, Giasson BI, Norris EH, Rueter SM, Trojanowski JQ, Lee VM, Ischiropoulos H (2001) Induction of alpha-synuclein aggregation by intracellular nitrative insult. J Neurosci 21(20):8053–8061
46. Duda JE, Giasson BI, Chen Q, Gur TL, Hurtig HI, Stern MB, Gollomp SM, Ischiropoulos H, Lee VM, Trojanowski JQ (2000) Widespread nitration of pathological inclusions in neurodegenerative synucleinopathies. Am J Pathol 157(5):1439–1445. doi:10.1016/S0002-9440(10)64781-5
47. Couch Y, Alvarez-Erviti L, Sibson NR, Wood MJ, Anthony DC (2011) The acute inflammatory response to intranigral alpha-synuclein differs significantly from intranigral lipopolysaccharide and is exacerbated by peripheral inflammation. J Neuroinflammation 8:166. doi:10.1186/1742-2094-8-166
48. Theodore S, Cao S, McLean PJ, Standaert DG (2008) Targeted overexpression of human alpha-synuclein triggers microglial activation and an adaptive immune response in a mouse model of Parkinson disease. J Neuropathol Exp Neurol 67(12):1149–1158. doi:10.1097/NEN.0b013e31818e5e99
49. Watson MB, Richter F, Lee SK, Gabby L, Wu J, Masliah E, Effros RB, Chesselet MF (2012) Regionally-specific microglial activation in young mice over-expressing human wildtype alpha-synuclein. Exp Neurol 237(2):318–334. doi:10.1016/j.expneurol.2012.06.025
50. Su X, Federoff HJ, Maguire-Zeiss KA (2009) Mutant alpha-synuclein overexpression mediates early proinflammatory activity. Neurotox Res 16(3):238–254. doi:10.1007/s12640-009-9053-x
51. Uversky VN, Li J, Bower K, Fink AL (2002) Synergistic effects of pesticides and metals on the fibrillation of alpha-synuclein: implications for Parkinson's disease. Neurotoxicology 23(4–5):527–536
52. Betarbet R, Sherer TB, MacKenzie G, Garcia-Osuna M, Panov AV, Greenamyre JT (2000) Chronic systemic pesticide exposure reproduces features of Parkinson's disease. Nat Neurosci 3(12):1301–1306
53. Horowitz MP, Milanese C, Di Maio R, Hu X, Montero LM, Sanders LH, Tapias V, Sepe S, van Cappellen WA, Burton EA, Greenamyre JT, Mastroberardino PG (2011) Single-cell redox imaging demonstrates a distinctive response of dopaminergic neurons to oxidative insults. Antioxid Redox Signal 15(4):855–871. doi:10.1089/ars.2010.3629
54. Cannon JR, Geghman KD, Tapias V, Sew T, Dail MK, Li C, Greenamyre JT (2013) Expression of human E46K-mutated alpha-synuclein in BAC-transgenic rats replicates early-stage Parkinson's disease features and enhances vulnerability to mitochondrial impairment. Exp Neurol 240:44–56. doi:10.1016/j.expneurol.2012.11.007
55. Lee JW, Tapias V, Di Maio R, Greenamyre JT, Cannon JR (2015) Behavioral, neurochemical, and pathologic alterations in bacterial artificial chromosome transgenic G2019S leucine-rich repeated kinase 2 rats. Neurobiol Aging 36(1):505–518. doi:10.1016/j.neurobiolaging.2014.07.011
56. Sai Y, Chen J, Ye F, Zhao Y, Zou Z, Cao J, Dong Z (2013) Dopamine release suppression dependent on an increase of intracellular Ca(2+) contributed to rotenone-induced neurotoxicity in PC12 cells. J Toxicol Pathol 26(2):149–157. doi:10.1293/tox.26.149
57. Arnold B, Cassady SJ, VanLaar VS, Berman SB (2011) Integrating multiple aspects of mitochondrial dynamics in neurons: age-related differences and dynamic changes in a chronic rotenone model. Neurobiol Dis 41(1):189–200. doi:10.1016/j.nbd.2010.09.006
58. Gao HM, Liu B, Hong JS (2003) Critical role for microglial NADPH oxidase in rotenone-induced degeneration of dopaminergic neurons. J Neurosci 23(15):6181–6187
59. Gonzalez-Hernandez T, Rodriguez M (2000) Compartmental organization and chemical profile of dopaminergic and

GABAergic neurons in the substantia nigra of the rat. J Comp Neurol 421(1):107–135
60. Bredt DS, Glatt CE, Hwang PM, Fotuhi M, Dawson TM, Snyder SH (1991) Nitric oxide synthase protein and mRNA are discretely localized in neuronal populations of the mammalian CNS together with NADPH diaphorase. Neuron 7(4):615–624
61. Liberatore GT, Jackson-Lewis V, Vukosavic S, Mandir AS, Vila M, McAuliffe WG, Dawson VL, Dawson TM, Przedborski S (1999) Inducible nitric oxide synthase stimulates dopaminergic neurodegeneration in the MPTP model of Parkinson disease. Nat Med 5(12):1403–1409. doi:10.1038/70978
62. Dryanovski DI, Guzman JN, Xie Z, Galteri DJ, Volpicelli-Daley LA, Lee VM, Miller RJ, Schumacker PT, Surmeier DJ (2013) Calcium entry and alpha-synuclein inclusions elevate dendritic mitochondrial oxidant stress in dopaminergic neurons. J Neurosci 33(24):10154–10164. doi:10.1523/JNEUROSCI.5311-12.2013
63. Giasson BI, Murray IV, Trojanowski JQ, Lee VM (2001) A hydrophobic stretch of 12 amino acid residues in the middle of alpha-synuclein is essential for filament assembly. J Biol Chem 276(4):2380–2386. doi:10.1074/jbc.M008919200
64. Diers AR, Higdon AN, Ricart KC, Johnson MS, Agarwal A, Kalyanaraman B, Landar A, Darley-Usmar VM (2010) Mitochondrial targeting of the electrophilic lipid 15-deoxy-Delta 12,14-prostaglandin J2 increases apoptotic efficacy via redox cell signalling mechanisms. Biochem J 426(1):31–41. doi:10.1042/BJ20091293